https://doi.org/10.5194/egusphere-2026-2791
Preprint. Discussion started: 9 July 2026
© Author(s) 2026. CC BY 4.0 License.

Geological controls on the formation and evolution of shoreface-connected ridges: new insights from the Stroombank sand ridge (Belgian coast)

Víctor Cartelle[1], Soetkin Vervust[2], Thomas Mestdagh[1], Wout Van Wesemael[3,4], Yağız Arda Çiçek[5], Christian Schwarz[5,6], Tine Missiaen[1], Tim Kinnaird[7], Ruth Plets[1]

[1]Flanders Marine Institute (VLIZ), Jacobsenstraat 1, 8400, Oostende, Belgium
[2]Vrije Universiteit Brussel, Archaeology, Environmental Changes, and Geo-Chemistry (AMGC), Pleinlaan 2, 1050, Brussels, Belgium
[3]KU Leuven, Faculty of Medicine, Department of Oral Health Sciences, Kapucijnenvoer 7, 3000, Leuven, Belgium
[4]KU Leuven, Faculty of Engineering Science, Department of Materials Engineering, Kasteelpark Arenberg 44, 3001, Leuven, Belgium
[5]KU Leuven, Department of Civil Engineering, Kasteelpark Arenberg 40, 3001, Leuven, Belgium
[6]KU Leuven, Department of Earth and Environmental Sciences, Celestijnenlaan 200E, 3001, Leuven, Belgium
[7]University of St Andrews, School of Earth and Environmental Sciences, Bute Building, Queen's Terrace, St Andrews, KY16 9TS, United Kingdom

Correspondence to: Víctor Cartelle (victor.cartelle@vliz.be)

Abstract. Shoreface-connected ridges are large bedforms of the lower shoreface that play a key role in sediment redistribution between the shelf and the coast, yet their origin and long-term dynamics remain debated and poorly constrained due to limited geological information. Here we integrate high-resolution acoustic data, sedimentological analyses, and new radiocarbon and optically stimulated luminescence dates to reconstruct the origin and evolution of the Stroombank, a shoreface-connected ridge on the Belgian continental shelf. The ridge consists of landward-dipping clinoforms overlying an irregular basal disconformity that locally truncates Pleistocene and Holocene deposits. Chronological constraints indicate that ridge development began ca. 1.3 ka ago, followed by sustained shore-parallel elongation and landward migration. We infer that initial ridge formation was fuelled by sediment derived from a waning late-Holocene tidal inlet, after which elongation and migration were maintained through sediment distribution within the active shoreface. We propose a formation model in which wave-driven cross-shore transport, combined with flood-dominant residual sediment transport, explains the coupled landward migration and alongshore elongation reconstructed in the internal architecture. The Stroombank is therefore interpreted as an actively evolving sedimentary body rather than a relict feature. This interpretation is supported by the coexistence of active and inactive (preserved) sectors within the ridge. The preserved inactive sector allowed us to date the inception of the ridge, while the occurrence of both active and inactive sectors indicates that ridge development is spatially heterogeneous and reflects a continuum from antecedent to active phases. These results demonstrate that shoreface-connected ridges can form composite geomorphic features controlled by the interplay of

https://doi.org/10.5194/egusphere-2026-2791
Preprint. Discussion started: 9 July 2026
© Author(s) 2026. CC BY 4.0 License.

sediment supply, hydrodynamic forcing and shoreface retreat, and provide geological constraints to evaluate existing conceptual and process-based models of ridge formation and evolution.

1 Introduction

Shoreface-connected ridges (SFCR) are offshore undulating bedforms attached to the adjacent coast, found on shallow continental shelves, usually displaying crestline orientation angles of 25-35° relative to the coastline (Dyer and Huntley, 1999). They are typically up to 10 m high, 2-5 km apart and can extend for tens of kilometres. These ridges are observed in many tide- and storm-dominated shelves around the world in depths of 10-20 m (Swift et al., 1978), such as the Atlantic coast of North America (Dalrymple and Hoogendoorn, 1997; Goff, 2014; Nnafie et al., 2014, 2015; Pendleton et al., 2017; Swift and Field, 1981), South America (Muñoz et al., 2013; Parker et al., 1982), South Africa (Cawthra et al., 2012) and Europe (the North Sea, Antia, 1996; van de Meene and van Rijn, 2000a; Nnafie et al., 2024; Verwaest et al., 2022).

The dominant hypothesis for the origin and evolution of shoreface-connected ridges relates their formation to tidal inlet and barrier retreat. Specifically, it is hypothesized that sand derived primarily from ebb-tidal delta deposits is remobilised by storm-induced flows during shoreline retreat, leading to ridge formation (Dyer and Huntley, 1999; McBride and Moslow, 1991; Snedden et al., 1994). The oblique orientation and linear shape of the SFCRs are attributed to shoreline transgression, lateral inlet migration and wave-driven reworking along a retreating ebb-tidal delta (McBride and Moslow, 1991). Numerical modelling studies by Trowbridge (1995) and Calvete et al. (2001) further indicate that the morphology of SFCRs is likely controlled by hydrodynamic processes during storms, which can account for their persistence and migration. However, recent modelling research using idealised schematisations has been able to produce self-generating shoreface-connected ridges in centennial timescales by including only wave processes and randomly imposed bottom perturbations (Dujardin et al., 2024). These findings exclude the requirement of sea-level rise and coastal retreat, resurfacing an old debate about the origin and formation of SFCRs (Dyer and Huntley, 1999; McBride and Moslow, 1991). As a result, it remains unclear to what extent these ridges represent primarily antecedent, transgression-related features reworked by contemporary processes, or whether they can emerge and persist solely through present-day hydrodynamic forcing.

Uncertainty about the origin and evolution of these ridges is linked to the limited understanding of lower shoreface morphodynamics in general (Anthony and Aagaard, 2020). Shoreface-connected ridges appear to play a potentially important role in modulating shoreface equilibrium, as they are associated with both shoreward and seaward sediment mobilisation. Numerical modelling studies have suggested that SFCRs may promote coastal progradation where the ridge crest attaches to the shoreline, while simultaneously enhancing coastal retreat in the adjacent trough located between the ridge and the coast (Nnafie et al., 2024; Safak et al., 2017). Field-based observational studies have reported evidence for net onshore-directed sediment fluxes associated with these ridges, implying a contribution to coastal stability and protection

https://doi.org/10.5194/egusphere-2026-2791
Preprint. Discussion started: 9 July 2026
© Author(s) 2026. CC BY 4.0 License.

(Hequette and Aernouts, 2010; Schwab et al., 2014; Verwaest et al., 2020). However, this sediment contribution to the coast has also been questioned (Kana et al., 2011), and some observations during intense storm events indicate net offshore sand transport (Goff et al., 2015). Furthermore, Goff (2014) proposed that ridge migration may actively contribute to shoreface ravinement, generating a stratigraphically recognisable erosional surface beneath the ridge. Taken together, these contrasting interpretations highlight that the influence of SFCRs on shoreline behaviour remains unresolved. Importantly, most insights into their long-term coastal impact derive from idealised numerical modelling approaches (Nnafie et al., 2014, e.g., 2024; Safak et al., 2017), whereas direct observations are generally restricted to short time spans and event-scale measurements. Such datasets, often limited to historical periods and potentially influenced by human interventions, may not adequately capture the natural, centennial-to-millennial scale ridge-coast interactions.

Detailed geological studies of SFCRs are scarce, yet these may provide an important piece in understanding their long-term evolution, origin and impact on the shoreface. Early work by Swift and Field (1981) and Parker et al. (1982) documented ridge morphology, surface grain-size and bedform patterns, and their association with storm-dominated settings. Subsequent seismic and core-based investigations (e.g., Dalrymple and Hoogendoorn, 1997; Snedden et al., 1994) revealed internal stratigraphic architectures consistent with episodic reworking and active migration. More recent studies integrating high-resolution geophysics (Schwab et al., 2000, 2013, 2014) investigated the interaction of the ridges and the shoreface. Despite these advances, detailed chronostratigraphic studies on ridge initiation and long-term migration pathways remain limited.

Here we provide a detailed geological study of the Stroombank, a shoreface-connected ridge offshore of the Belgian coast. In recent years, the Stroombank has been extensively studied using idealized modelling (Nnafie et al., 2021, 2024) and historical reconstructions based on 19th and 20th century bathymetric maps (Dujardin et al., 2024), an effort linked to the need for optimised coastal management by authorities in the face of increasing sea-level rise. Here, we reconstruct the internal architecture, chronology, and evolutionary trajectory of the ridge by integrating high-resolution geophysics, sedimentological data, and radiocarbon and optically stimulated luminescence dating. This approach allows us to identify the dominant controls on ridge development and to provide new geological constraints on the mechanisms governing their formation and persistence. In doing so, we assess to what extent existing conceptual and process-based models are consistent with the geological record and discuss the implications for current hypotheses on the origin and evolution of SFCRs.

2 Study area

The study area is located along the Belgian central and west coast, in the southern North Sea, reaching from the Belgian-French border in the southwest to the city of Oostende in the northeast (Fig. 1). It is a stretch of more than 30 km of straight coastline, heavily altered by human activities and infrastructure, including seawalls with integrated promenades, ports (Nieuwpoort and Oostende) and large shore-perpendicular groins. The coast is characterised by a macro-tidal regime with a

https://doi.org/10.5194/egusphere-2026-2791
Preprint. Discussion started: 9 July 2026
© Author(s) 2026. CC BY 4.0 License.

mean tidal range of 4 m, and an average significant wave height of 60 cm, exceeding 2 m 10% of the time (Verwaest et al., 2022). Sediment transport along this part of the Belgian coast is predominantly driven by residual tidal fluxes and a north-eastward oriented littoral drift. Cross-shore sediment transport is more variable, with both landward and seaward components depending on the distance from the shoreline, which are mainly driven by wave forcing (Dujardin et al., 2023, 2024). The shallow subtidal area is characterised by a swale and ridge morphology of large shoreface-connected ridges, with the Trapegeer-Broers-Den Oever banks in the west and the Stroombank ridge to the east.

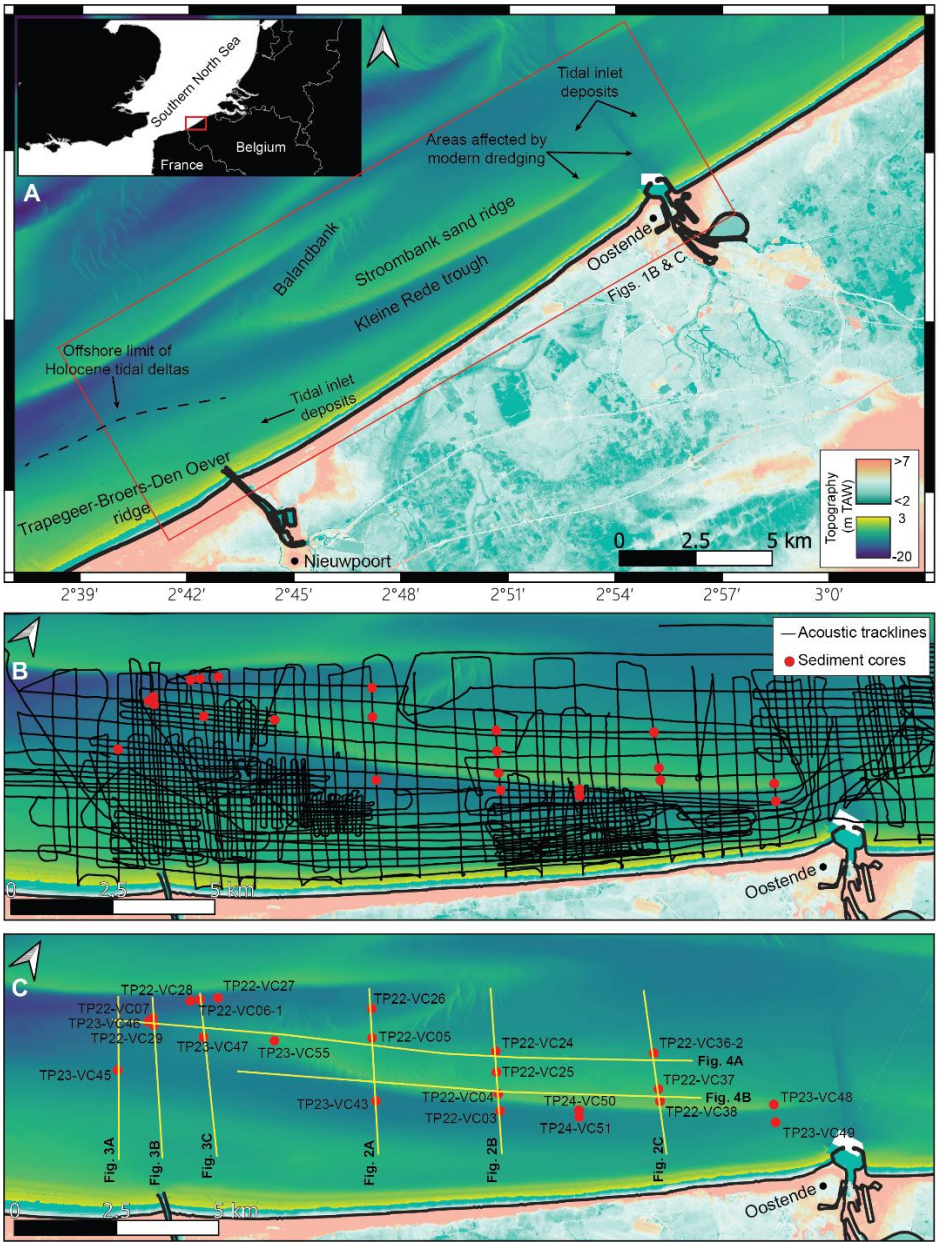

https://doi.org/10.5194/egusphere-2026-2791
Preprint. Discussion started: 9 July 2026
© Author(s) 2026. CC BY 4.0 License.

Figure 1. A) Location of the study area on the Belgian Middle coast, showing the main cities and the offshore location of deposits from Holocene tidal inlets and deltas identified by Cartelle et al. (2025) and Cartelle et al. (2026). B) Overview of all data collected in the study area, including high-resolution acoustic profiles and vibrocores. C) Detailed location of the sediment cores and the acoustic profiles shown on subsequent figures. Note that B and C have a different orientation than A. Background bathymetric data were provided by Agentschap Maritieme Dienstverlening en Kust and are available at www.agentschapmdk.be. Topographic data were provided by Nationaal Geografisch Instituut and are available at www.geo.be.

The Stroombank is a shoreface-connected sand ridge with a southwest to northeast crest-line orientation, almost parallel to the present-day coastline, at an angle of 8 degrees (Fig. 1). It is ca. 20 km long with a variable width, averaging ca. 1 km. It has a 3-km-long minor bank attached to it on its northwest offshore flank with a southwest to northeast orientation, known as the Balandbank. Between the Stroombank and the coastline, an elongated trough, known as the Kleine Rede, runs parallel to the ridge crest. The cross-section of the ridge is asymmetrical, with a gentle (ca. 0.1°) slope on the offshore flank and a steeper (up to 3.3°) slope in the landward direction. Shallowest depths at the ridge crest reach up to -4.5 m MSL (mean sea level). The trough has depths ranging from -7.9 to -12.3 m MSL, deepening from northeast to southwest, as it becomes wider. The Stroombank attaches to the coast 8 km to the northeast of Oostende. However, due to dredged channels cutting across the ridge to allow access to the port of Ostend, there is a disconnection between the northerly and southerly parts of the bank (Houthuys et al., 2021). This has disrupted the supply of sediment to the northeasterly part of the ridge from as early as 1880 (Houthuys et al., 2021).

Whilst the seabed is dominated by sand ridges, the subsurface geology is characterised by relatively thin and patchy Late Pleistocene and Holocene deposits (De Clercq, 2018; Mathys, 2009) that overlie thick Palaeogene units mainly composed of compacted, folded and faulted clays and sand to sandy clays (De Batist, 1989; Henriet and De Moor, 1989; Jacobs and De Batist, 1996). Recent studies in the nearshore area have revealed the presence of extensive deposits of former tidal inlets and ebb-tidal deltas, whose channel fills range in age from ca. 8 cal ka BP to the present (Cartelle et al., 2025, 2026). These are mainly preserved offshore of the cities of Nieuwpoort and Oostende (Fig. 1). They are associated with laterally continuous layers of peat found in the intertidal and shallow subtidal sectors between both cities (Cartelle et al., 2025; Missiaen et al., 2018). These deposits record a palaeogeographic configuration in which the coastline was located at least 2 km seaward of its present-day position and displayed a different orientation, forming an oblique angle of ~5° relative to the modern coastline (Cartelle et al., 2025, 2026).

3 Methods

Seismic and sedimentary data included here were collected during 10 offshore surveys onboard the RV *Simon Stevin* and the dive vessel *Last Freedom*, during the years 2022, 2023 and 2024. Each data type will be discussed below in greater detail.

https://doi.org/10.5194/egusphere-2026-2791
Preprint. Discussion started: 9 July 2026
© Author(s) 2026. CC BY 4.0 License.

3.1 Geophysical data

High-resolution acoustic data were collected with an Innomar SES-2000 Quattro parametric sub-bottom profiler operated in single-beam mode, using primary frequencies of 8 or 10 kHz. Horizontal positioning was provided by an RTK-GNSS system, and vessel motion was recorded by an external motion reference unit, allowing real-time heave correction. Raw data stored in Innomar's proprietary .ses3 format were converted to SEG-Y prior to processing. To remove vertical offsets related to tidal fluctuations, profiles were corrected in RadExPro and subsequently referenced to the Belgian vertical datum (TAW), equivalent to 2.3 m below mean sea level at Oostende. These profiles are shown in the figures in milliseconds two-way traveltime (ms TWT). Acoustic facies and stratigraphic units were interpreted following standard seismic-stratigraphic principles (Mitchum, 1977; Mitchum et al., 1977; Mitchum and Vail, 1977). Key horizons were mapped throughout the study area and interpolated using the flex gridding algorithm within S&P Global-Kingdom (v. 2023). The units bounded by the mapped horizons were characterised based on acoustic facies and validated against sediment cores collected at targeted locations. A constant P-wave velocity in sediment of 1600 m/s was applied for time-depth conversion. Where feasible, compaction effects were corrected by comparing core recovery to total penetration depth, and major lithological shifts were considered the main sources of acoustic impedance contrasts.

3.2 Sediment cores

Sediment sampling was carried out with a 3-m-long vibrocorer (Ocean Scientific International Ltd.) equipped with a 11.5 cm diameter steel barrel and a >100 kN vibrating head. Sediment cores were collected at 22 selected sites, for which the coordinates are provided in Table A1. Cores were split longitudinally under red light in the lab to store half of each section in light-safe conditions. After splitting, one half of the core was photographed and described. Grain size was recorded visually using a comparative grain-size chart, and selected samples underwent detailed particle-size analysis by laser diffraction (Malvern Mastersizer 3000) at Ghent University. Prior to analysis, samples were pre-treated with H_2O_2 and HCl to remove organic matter and carbonates. Grain-size terminology follows Wentworth (1922). Lithofacies were classified using the standard terminology of Farrell et al. (2012) (Table A2). Intervals with high-frequency alternations of mm–cm-scale beds and laminae were assigned to heterolithic facies.

3.3 Dating

Radiocarbon dating as well as optically stimulated luminescence (OSL) profiling and dating were used to establish the chronological context of the deposits identified offshore. A total of 10 samples were used for radiocarbon dating, including well-preserved valves without clear evidence of weathering, foraminifera and peat samples. Analyses were performed at Beta Analytic Laboratory (USA) and at the radiocarbon dating laboratory of the Royal Institute for Cultural Heritage of Belgium (KIK-IRPA). All radiocarbon dates are given in calibrated years before present (cal a BP, 2σ confidence level) after calibration using Calib Rev. 8.2 (Stuiver and Reimer, 1993). The Marine20 calibration curve (Heaton et al., 2020) has been

https://doi.org/10.5194/egusphere-2026-2791
Preprint. Discussion started: 9 July 2026
© Author(s) 2026. CC BY 4.0 License.

used for bivalve shells and foraminifera, and the IntCal20 calibration curve (Reimer et al., 2020) has been used for peat samples.

OSL profiling was performed on sand deposits at regular intervals along the cores following the methodologies described by Munyikwa et al. (2021) and Sanderson and Murphy (2010). A SUERC Portable OSL reader (Sanderson and Murphy, 2010) was used to measure luminescence signals from small (ca. 50 g) unprocessed bulk sediment samples using a standard continuous-wave (CW) proxies measurement sequence, acquiring infrared (IRSL) and blue post-IR OSL signals and depletion indices. The bulk luminescence signals (IRSL, OSL) are affected by multiple factors including the local dose rates, inherited luminescence at time of burial, luminescence sensitivity of the mineral grains, mineral composition and time since burial (Munyikwa et al., 2021; Sanderson and Murphy, 2010). Where these variables are broadly comparable between samples, signal intensity can be used as a relative age proxy, with higher intensities generally indicating older deposits. The resulting luminescence profiles were used to select the samples that would be further processed to obtain absolute OSL ages and to correlate deposits along and across the sand ridge.

OSL dating was performed at the School of Earth and Environmental Sciences of the University of St Andrews. Equivalent dose determination was made using the single aliquot regenerative dose (SAR) OSL protocol. The dose rates were assessed using a combination of low-level radioactivity measurements in the luminescence laboratory, and determination of radionuclide concentrations by mass spectrometry at X-Ray Mineral Services. Methodological details can be found in Supplementary Material. A total of 23 samples were subjected to absolute OSL dating.

4 Results and interpretation

4.1 Internal structure and sedimentary architecture

Geophysical profiles across and along the Stroombank reveal a well-defined internal architecture that distinguishes ridge deposits from overlying and underlying units, allowing the feature to be mapped as a coherent sedimentary body (Figs. 2, 3 and 4). Cross-shore profiles between Nieuwpoort and Oostende, where the Stroombank is clearly visible on the bathymetric data (Fig. 1), reveal that the ridge consists of an acoustic facies dominated by medium-amplitude, high-continuity oblique-tangential reflections that form gently dipping clinoform packages (Fig. 2). The profiles shown in Fig. 2 indicate that the ridge is composed of several superimposed clinoformal units forming a sedimentary body of variable width. Moving further southwards, the Stroombank is no longer discernible on the bathymetric data (Fig. 1) but can still be observed on the acoustic profiles (Fig. 3). Deposits in this sector are characterised by the same acoustic facies, with oblique-tangential reflections forming gently dipping clinoforms that are now buried underneath younger deposits. The preserved sedimentary body becomes narrower and thinner towards the southwest (Fig. 3). All profiles display a consistent apparent dip direction towards the landward side (Figs. 2 and 3).

https://doi.org/10.5194/egusphere-2026-2791
Preprint. Discussion started: 9 July 2026
© Author(s) 2026. CC BY 4.0 License.

On along-shore profiles, crossing both the buried southern and exposed northern sector of the Stroombank, the internal configuration is dominated by low-angle oblique-tangential reflections that downlap onto a basal surface (Fig. 4A). Locally, sigmoidal reflection geometries are also observed (Fig. 4B). The apparent dip direction varies along the ridge. In the southern sector, reflections locally indicate southwest-directed progradation, whereas northeast-directed progradation characterises most of the alongshore profiles (Fig. 4).

To quantify the overall orientation of internal accretion, the apparent dip directions measured on cross-shore (Figs. 2 and 3) and alongshore (Fig. 4) profiles were combined to calculate a net clinoform slope vector for each sector of the ridge. This approach integrates the orthogonal components of the dip derived from two profile orientations, allowing reconstruction of the three-dimensional direction of progradation. The resulting vectors (Fig. 5B) indicate an average net slope of approximately 3°, with azimuths ranging between 60° and 170° relative to the north. Despite this variability, all calculated vectors show a consistent landward-directed component for most of the ridge. Moreover, a systematic spatial pattern is observed: the net progradation direction rotates clockwise from the offshore flank towards the onshore sector of the ridge (Fig. 5B).

Mapping of the deposits associated with the ridge allows the basal surface to be traced as a distinct erosional disconformity with an irregular topography (Fig. 5A). Its depth varies markedly along the ridge: it reaches its maximum depth in the southwest, down to −20.2 m MSL, and becomes progressively shallower towards the northeast, where it rises to approximately −9.7 m MSL (Fig. 5A). In the cross-ridge direction, the morphology of the basal surface also changes systematically. The southwestern sector is underlain by a nearly flat, laterally continuous surface (Figs. 2A and 3), whereas the central sector displays a pronounced landward deepening associated with the stacked clinoformal packages that compose the ridge (Fig. 2B). Further to the northeast, this geometry shifts again and the basal surface flattens into a gently undulating horizon (Fig. 2C).

Beneath this basal disconformity, two main sedimentary units occur: a laterally continuous deposit and a discontinuous set of infills. The continuous unit is largely acoustically transparent and bounded at the top by a high-amplitude, irregular reflection (Fig. 3). These characteristics, together with its extensive distribution, are consistent with the pre-Quaternary clays previously mapped across the Belgian continental shelf (De Clercq et al., 2016). The discontinuous deposits display variable acoustic facies and are mostly confined to isolated pockets beneath the ridge in the southwest (labelled as Pleistocene deposits in Fig. 3), becoming thicker and more widespread towards the northeast (labelled as Holocene/Pleistocene deposits in Fig. 2).

The thickness distribution of the ridge mirrors the present-day bathymetry (Fig. 5B). The greatest sediment accumulation occurs along the ridge crest, where its thickness reaches up to 9.3 m. Ridge deposits gradually thin seawards and are sharply bounded landward by the Kleine Rede trough (Fig. 1). The thickness map demonstrates that the Stroombank ridge is a composite of two arcuate sedimentary bodies (the crest is indicated with dashed lines in Fig. 5B). The smaller ridge (phase I) located in the southwest is mostly buried (Fig. 3), while the larger ridge to the east (phase II) corresponds to the active sector of the Stroombank (Fig. 2). Their general crestline orientation differs by approximately 5 degrees (Fig. 5B).

https://doi.org/10.5194/egusphere-2026-2791
Preprint. Discussion started: 9 July 2026
© Author(s) 2026. CC BY 4.0 License.

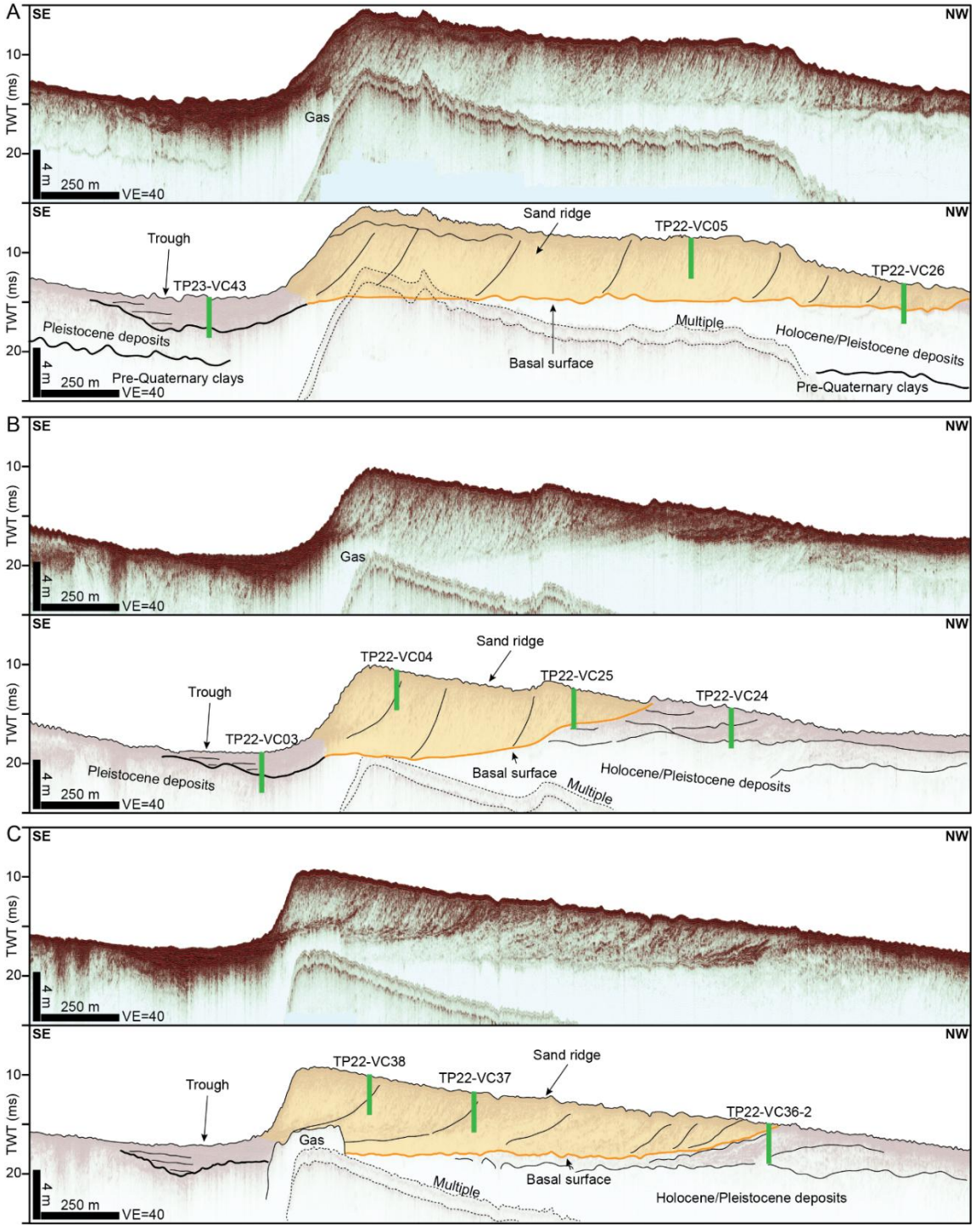

230 **Figure 2. High-resolution acoustic profiles across the active sector of the Stroombank sand ridge and the Kleine Rede trough, arranged from southwest to northeast (A–C). Profile locations are shown in Fig. 1C, and corresponding sediment cores are presented in Fig. 6.**

https://doi.org/10.5194/egusphere-2026-2791
Preprint. Discussion started: 9 July 2026
© Author(s) 2026. CC BY 4.0 License.

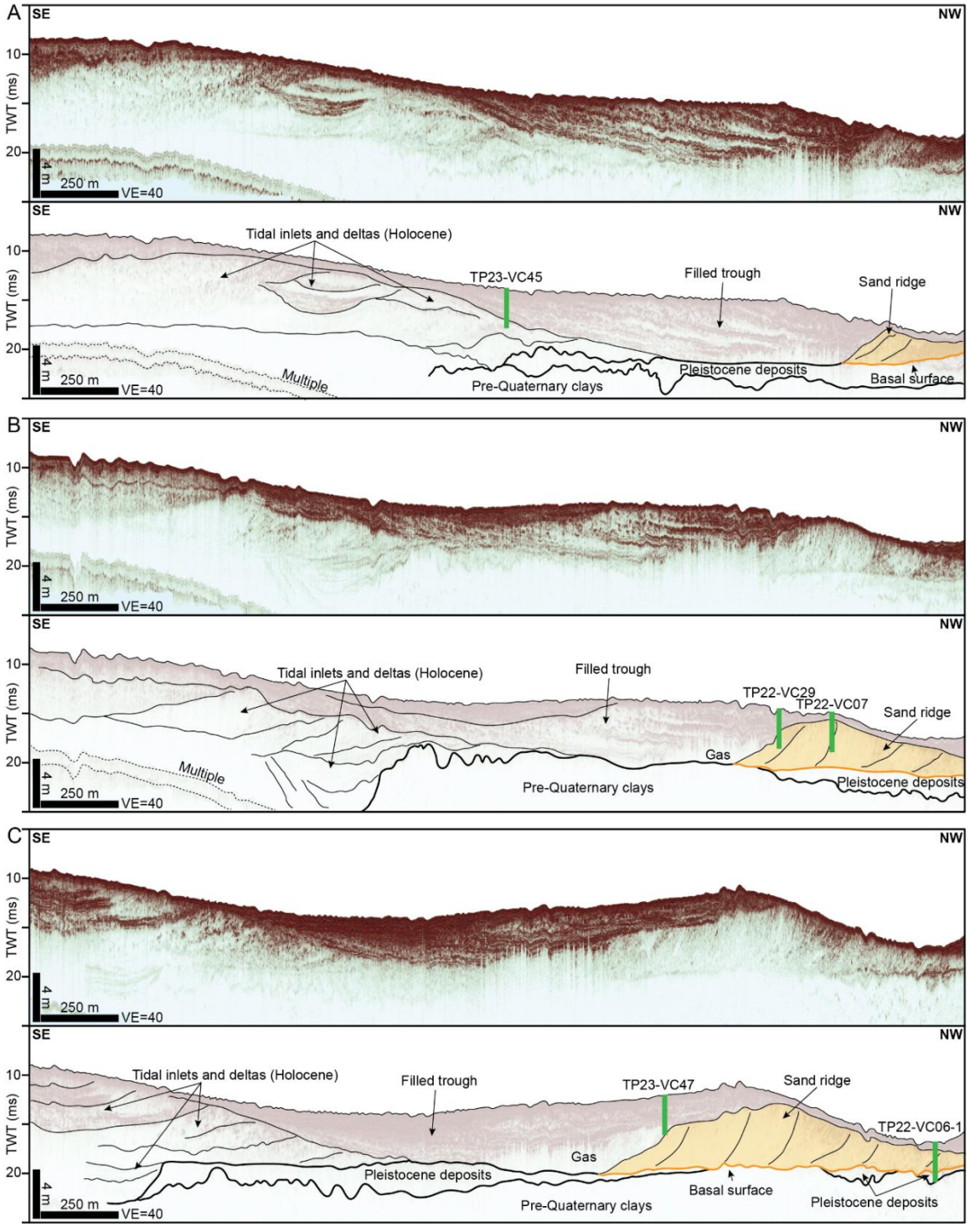

Figure 3. High-resolution acoustic profiles across the sand ridge in the sector where it is buried under younger deposits, arranged from southwest to northeast (A–C). Profile locations are shown in Fig. 1C, and corresponding sediment cores are presented in Fig. 6. Interpretation of the Holocene tidal-inlet and deltaic units follows Cartelle et al. (2025) and Cartelle et al. (2026).

https://doi.org/10.5194/egusphere-2026-2791
Preprint. Discussion started: 9 July 2026
© Author(s) 2026. CC BY 4.0 License.

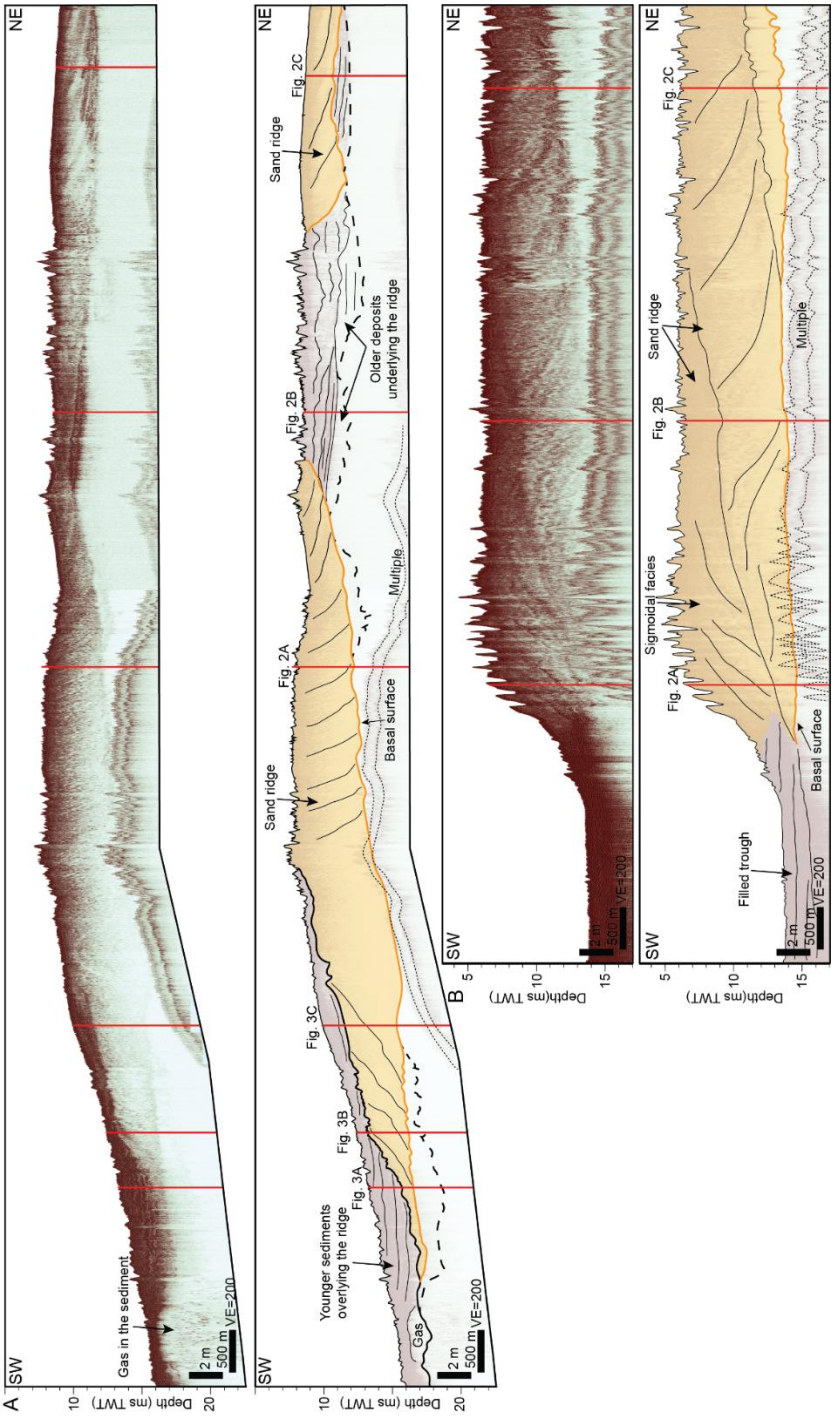

Figure 4. High-resolution acoustic profiles generated by merging multiple lines along the Stroombank sand ridge (SW to NE), displayed from offshore to onshore (A–B). Profile locations are shown in Fig. 1C, and corresponding sediment cores are presented in Fig. 6.

https://doi.org/10.5194/egusphere-2026-2791
Preprint. Discussion started: 9 July 2026
© Author(s) 2026. CC BY 4.0 License.

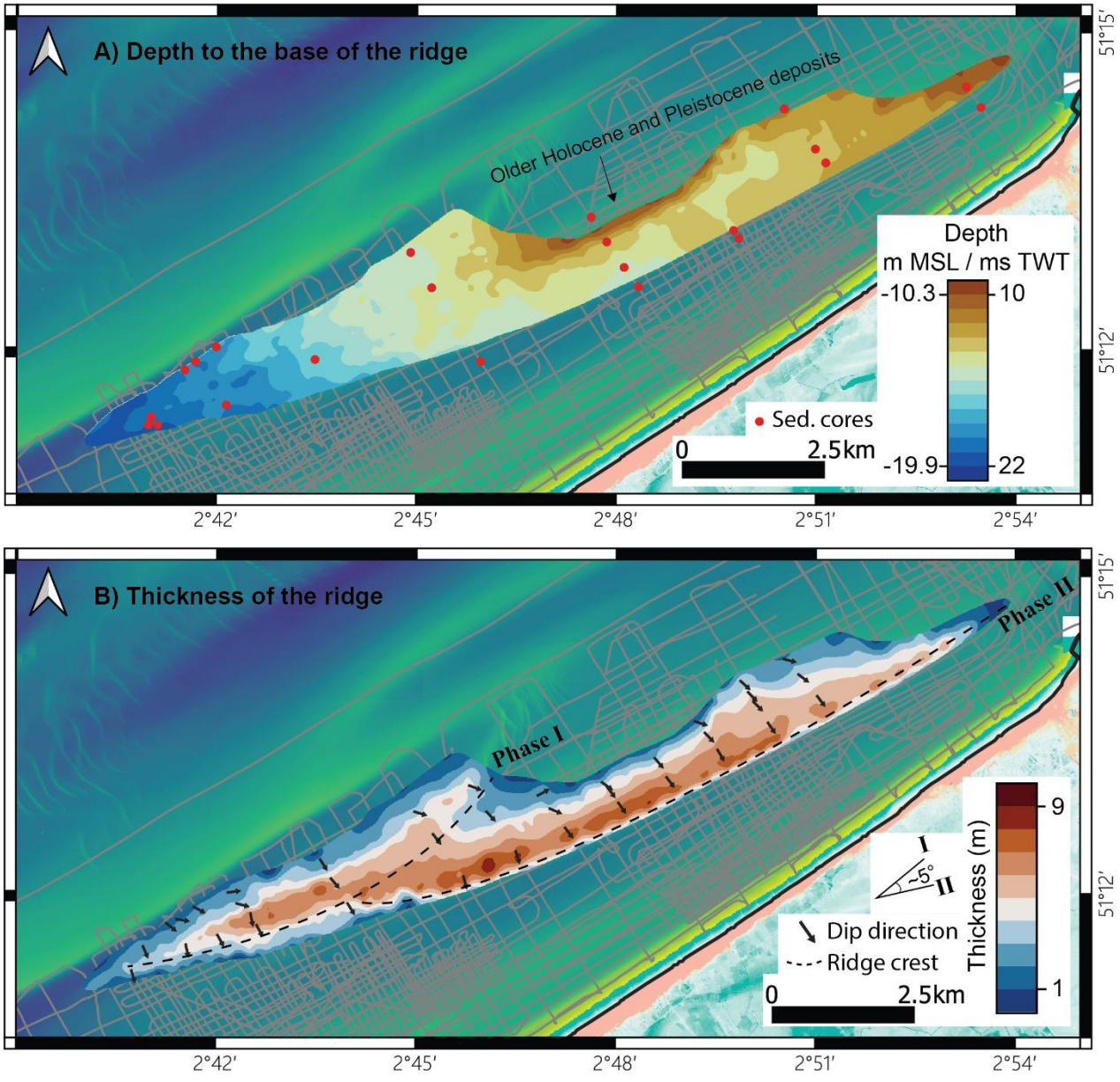

Figure 5. (A) Map of the depth to the basal disconformity underlying the Stroombank sand-ridge deposits. (B) Thickness map of the sedimentary body forming the Stroombank sand ridge. Phases I and II represent two stages of the ridge development, with phase I mostly buried and phase II corresponding to the present-day Stroombank ridge. Background bathymetric data were provided by Agentschap Maritieme Dienstverlening en Kust and are available at www.agentschapmdk.be. Topographic data were provided by Nationaal Geografisch Instituut and are available at www.geo.be.

The Kleine Rede forms a pronounced trough running parallel to and landward of the Stroombank, with present-day depths between −7.9 and −12.3 m MSL (Fig. 1). Geophysical profiles also show a distinct infilling pattern with horizontal

https://doi.org/10.5194/egusphere-2026-2791
Preprint. Discussion started: 9 July 2026
© Author(s) 2026. CC BY 4.0 License.

reflections onlapping onto the basal disconformity in the landward direction and interfingered with the clinoforms of the sand ridge in a seaward direction (Figs. 2 and 4). Localised acoustic blanking obscures parts of the basal surface, particularly across the transition zone between the trough and the ridge, limiting detailed mapping in these sectors (Figs. 2 and 3). The trough fill is characterised by high-amplitude, laterally continuous reflections, with amplitudes exceeding those of the main ridge deposits. Towards the southwest, the Kleine Rede becomes less confined by the trough morphology, and its sedimentary infill widens and thickens, merging laterally with broader shoreface deposits and overtopping the ridge (Fig. 3).

4.2 Sedimentary facies

The sedimentary facies of the Stroombank sand ridge show a dominance of laminated fine to medium sand (S_{lam}) recovered from the clinoform sets (Figs. 6 and 7). This sediment contains abundant shells, shell fragments and other remains of marine fauna (such as sponge spicules, sea urchin spines or foraminifera), with some cores showing slightly coarser sand with abundant shell fragments (mxd gS_{lam}, e.g., core TP22-VC38, Fig. 6). In general, the sand is homogeneous, with D50 values ranging from 201 to 358 µm, with average values of 258 µm. In some cases, interbedded muds and sands are found at the base of the cores ($S_{lam}/M_{m\text{-}org}$) and correspond to areas with higher-amplitude reflections in the geophysical data (e.g., core TP22-VC04, Fig. 2B and 6, transect B). Some cores reached the basal disconformity, indicating the presence of mixed (bioclastic and siliciclastic) gravel deposits (mxd msG-m) with abundant large shells and shell fragments, pebble and cobble-sized rock fragments and clay chunks (e.g., cores TP22-VC06-1 and TP22-VC26, Figs. 2A, 3C, 6 -transects A and D- and 7). The sediments underneath the disconformity either correspond to laminated fine sands (S_{lam}) or very stiff grey clay (C_m).

The Kleine Rede trough is mostly characterised by organic-rich muddy sediments ($sM_{lam\text{-}org}$, e.g., cores TP22-VC03 and TP23-VC49, Figs. 6 -transect B- and 7), sometimes with some intercalations of distinct sand laminations (mS_{lam}, $M/S_{lam\text{-}biot}$, e.g., core TP24-VC51, Fig. 6, transect D). To the southwest, the lithofacies of the Kleine Rede show a clear change as the sediments become sandier, with laminated sand ($S_{lam\text{-}gr}$, core TP23-VC45, Fig. 6, transect D). These sedimentary facies are similar to those found in the deposits overlying the Stroombank sand ridge in the southwestern sector. These generally correspond to structureless or laminated fine to medium sands (S_m, S_{lam}) with some basal or intercalated shell-rich gravel deposits (mxd $sG\text{-}c_{lam}$, mxd msG-m) (e.g., cores TP22-VC29 and TP23-VC47, Fig. 6, transect D).

https://doi.org/10.5194/egusphere-2026-2791
Preprint. Discussion started: 9 July 2026
© Author(s) 2026. CC BY 4.0 License.

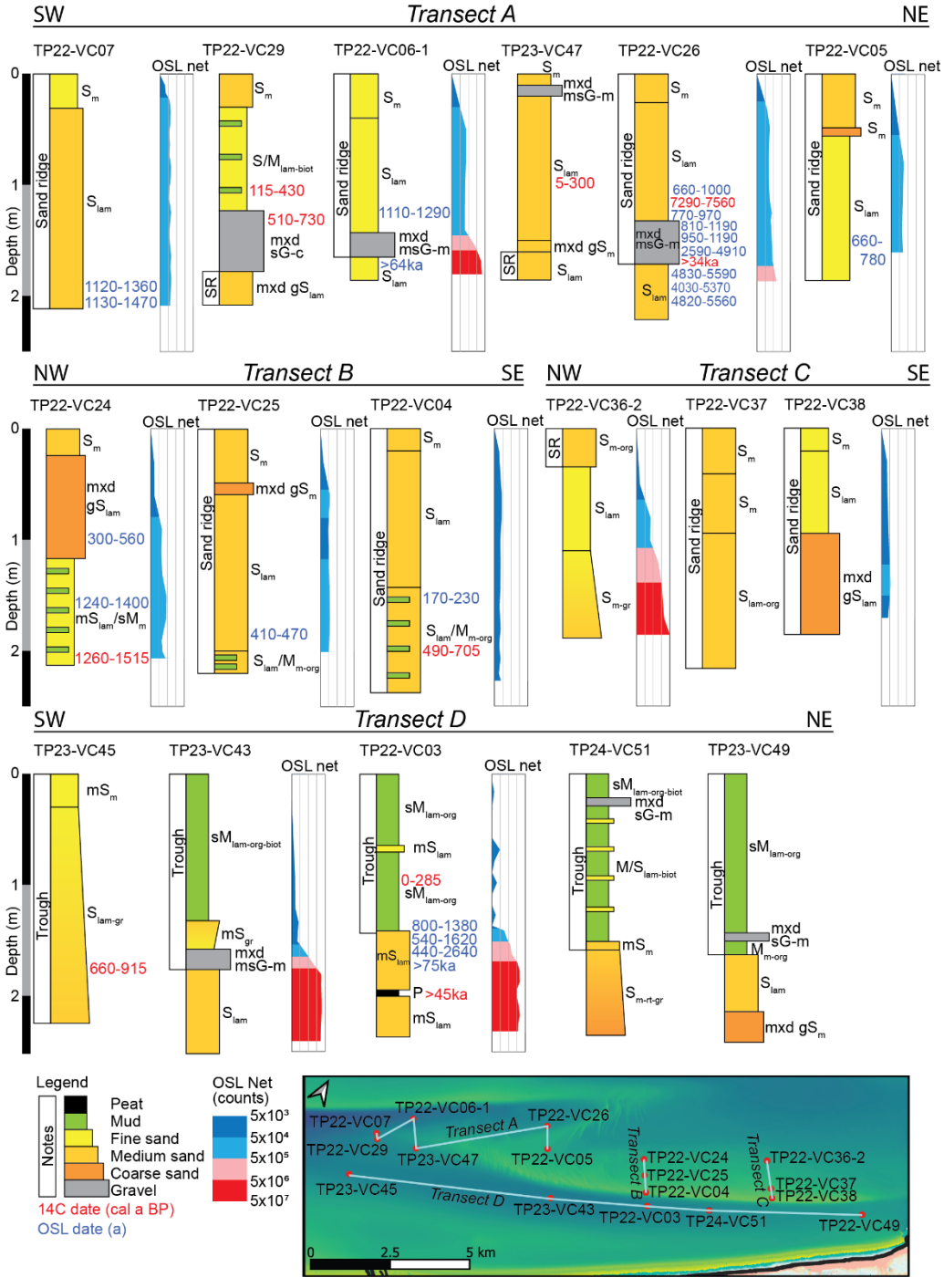

Figure 6. Representative sediment cores from the Stroombank sand ridge and the Kleine Rede trough, grouped into four transects. Transect A illustrates cores along the offshore flank of the ridge (southwest to northeast). Transects B and C display cross-shore sections through the ridge from offshore to onshore. Transect D presents cores acquired along the Kleine Rede trough. Additional core logs are included in Fig. A1. OSL profiling results are shown in simplified form when available (in counts); detailed luminescence data are provided in Supplementary Material. For the sedimentary facies codes, refer to Table A2. Background

https://doi.org/10.5194/egusphere-2026-2791
Preprint. Discussion started: 9 July 2026
© Author(s) 2026. CC BY 4.0 License.

bathymetric data were provided by Agentschap Maritieme Dienstverlening en Kust and are available at www.agentschapmdk.be. Topographic data were provided by Nationaal Geografisch Instituut and are available at www.geo.be.

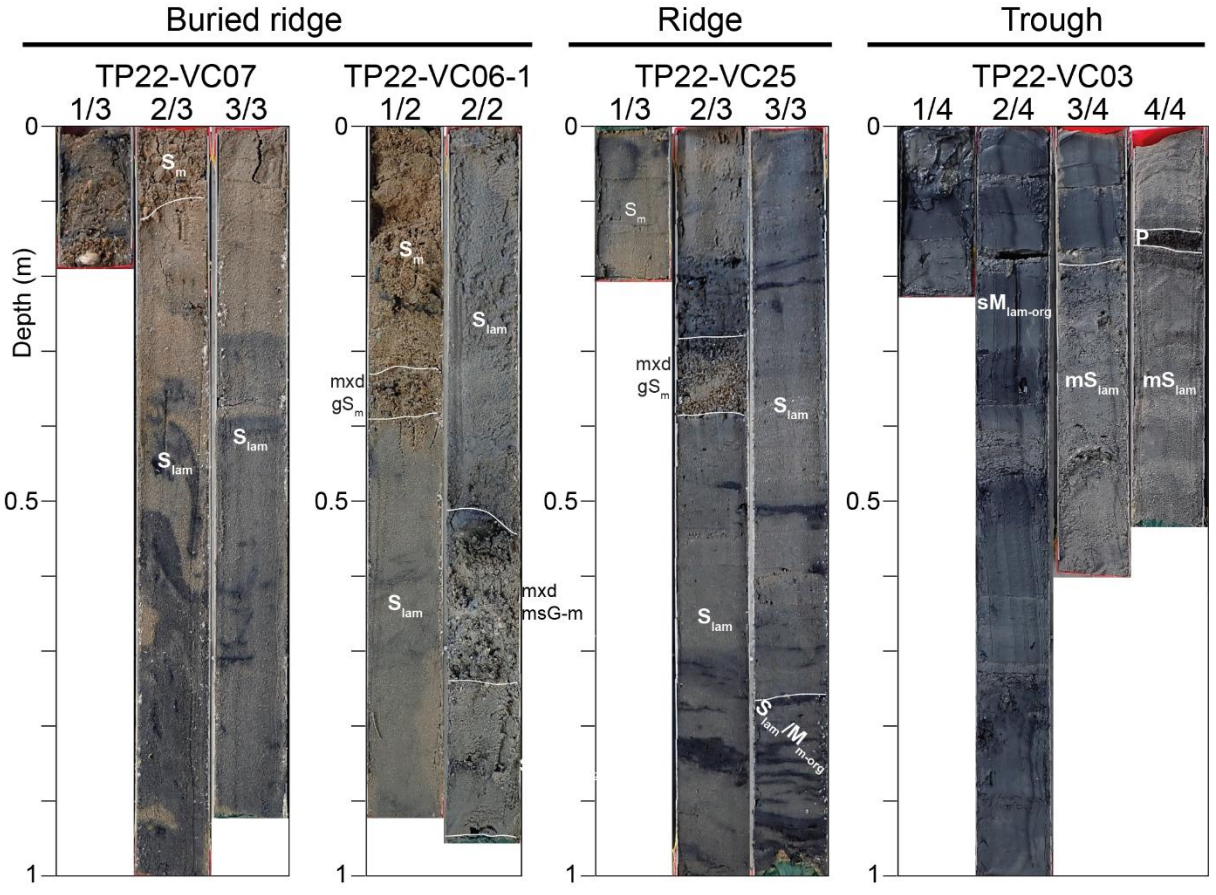

Figure 7. Representative pictures of sediment cores recovered from the buried ridge, the active ridge and the trough. For the sedimentary facies codes, refer to Table A2.

4.3 Luminescence profiling

Luminescence profiling was carried out on twelve selected cores distributed along and across the Stroombank sand ridge, as well as on several cores recovered from the Kleine Rede trough. Cores that penetrated to the basal disconformity, whether within the ridge or within the trough, show the widest range of luminescence intensities (expressed as net OSL counts, counted over 60 s), with values increasing from $<5 \times 10^4$ counts near the top to $>5 \times 10^6$ counts at depth (e.g., TP22-VC06-1 and TP22-VC03, Fig. 6).

Across the main ridge deposits, luminescence signals display a consistent spatial pattern. Cores located further offshore or towards the southwestern part of the ridge (e.g., TP22-VC06-1, TP22-VC26) show the highest luminescence values (from ~5 $\times 10^4$ to ~5 $\times 10^5$ counts, Fig. 6), whereas cores from the ridge crest (e.g., TP22-VC04) yield the lowest intensities ($<5 \times 10^4$ counts, Fig. 6). This highlights a trend of decreasing luminescence intensities from southwest to northeast. Given the broadly

https://doi.org/10.5194/egusphere-2026-2791
Preprint. Discussion started: 9 July 2026
© Author(s) 2026. CC BY 4.0 License.

homogeneous grain size and mineralogy across the ridge (Sect. 4.2), this trend is interpreted as reflecting decreasing ages (Munyikwa et al., 2021) from southwest to northeast across the ridge.

The Kleine Rede trough deposits also show a characteristic signature: the upper muddy sediments consistently produce very low luminescence values (<5 × 10^4 counts, Fig. 6), while the underlying sands record some of the highest intensities in the study area (>5 × 10^6 counts, Fig. 6), indicating a large age gap between these upper and lower deposits.

Luminescence profiles were used to guide the selection of samples for absolute OSL dating. To capture the full range of stratigraphic units, we targeted horizons representing different orders of magnitude of luminescence intensity (i.e. 10^3, 10^4, 10^5, 10^6 counts), focusing on cores TP22-VC03, TP22-VC04, TP22-VC05, TP22-VC06-1, TP22-VC07, TP22-VC24, TP22-VC25 and TP22-VC26 (Table 1, Fig. 6).

4.4 Dating

A total of 23 OSL ages and 9 radiocarbon ages were obtained (Table 1), with both methods yielding consistent chronologies for equivalent deposits (e.g., cores TP22-VC24 and TP22-VC04, Fig. 6). The oldest ages correspond to sandy units lying beneath the basal disconformity, which show a wide (OSL) age range from 63900-133300 a in core TP22-VC06-1 to 4030-5370 a in core TP22-VC26 (Table 1, Fig. 6). The oldest OSL age, despite its large uncertainty, indicates a Pleistocene origin and is associated with the highest luminescence signals in the dataset (>1 × 10^7 counts). This is concordant with the sample from TP22-VC03, which yielded an age of 74900-91300 a (Table 1, Fig. 6). These results suggest that other units with similarly high luminescence signals, such as the basal intervals of TP22-VC36-2 and TP23-VC43, likely represent Pleistocene deposits.

Table 1. Radiocarbon and OSL dates.

Radiocarbon dates							
Core	**Depth (cm)**	**Lab code**	**Material dated**	**Conventional radiocarbon age**	**Median probability (cal ka BP)**	**Calibrated age (cal a BP)**	**Feature dated**
TP22-VC03	95	Beta-665311	Marine shell (*Spisula* sp.)	710±30	0.18	0-285	Trough filling
TP22-VC03	196.5 - 199	RICH-35144	Peat	52700±2390	-	-*1	Deposits beneath the disconformity
TP22-VC04	200	RICH-35145	Shell (*Spisula* sp.)	1190±30	0.60	490-705	Sand ridge, clinoforms
TP22-VC24	211.5	RICH-35150	Shell (*Donax* sp.)	1980±30	1.37	1260-1515	Deposits beneath the disconformity
TP22-VC26	128	Beta-665307	Mixed foraminifera	7120±30	7.42	7290 – 7560*2	Sand ridge, clinoforms
TP22-VC26	167	RICH-35158	Shell (*Cerastoderma* sp.)	31520±136	35.12	34720 – 35440*2	Sand ridge, gravel lag

https://doi.org/10.5194/egusphere-2026-2791
Preprint. Discussion started: 9 July 2026
© Author(s) 2026. CC BY 4.0 License.

TP22-VC29	105	RICH-35151	Shell (*Cerastoderma* sp.)	810±30	0.27	115-430	Deposits above the buried ridge
TP22-VC29	134	RICH-35152	Shell (*Spisula* sp.)	1220±30	0.62	510-730	Deposits above the buried ridge
TP23-VC45	175	RICH-35156	Shell (*Spisula* sp.)	1400±30	0.79	660-915	Trough filling
TP23-VC47	97.5	RICH-35157	Shell (*Spisula* sp.)	720±30	0.18	5-300	Deposits above the buried ridge
Samples marked with * are considered reworked and therefore represent minimum ages. 1. Transported peat fragment. 2. Rejected based on luminescence results.							
Luminescence dates							
Core	**Depth**	**Lab code**	**Burial dose (Gy)**	**Total effective dose rate (mGy a^{-1})**	**Age (ka)**	**Age range (a, ±σ)**	**Feature dated**
TP22-VC03	141	CERSA 1202-15	0.97 ± 0.21	0.89 ± 0.14	1.09 ± 0.29	800-1380	Deposits beneath the disconformity
TP22-VC03	148	CERSA 1202-16	0.96 ± 0.46	0.89 ± 0.14	1.08 ± 0.54*	540-1620	Deposits beneath the disconformity
TP22-VC03	154	CERSA 1202-17	1.36 ± 0.97	0.89 ± 0.05	1.54 ± 1.10*	440-2640	Deposits beneath the disconformity
TP22-VC03	170	CERSA 1202-19	51.54 ± 2.92	0.62 ± 0.05	83.13 ± 8.20	74900-91300	Deposits beneath the disconformity
TP22-VC04	152	CERSA 1574	0.17 ± 0.03	0.82 ± 0.03	0.20 ± 0.03	170-230	Sand ridge, clinoforms
TP22-VC05	150	CERSA 1575	0.72 ± 0.05	1.00 ± 0.04	0.72 ± 0.06	660-780	Sand ridge, clinoforms
TP22-VC06	125	CERSA 1576	1.12 ± 0.04	0.93 ± 0.06	1.20 ± 0.09	1110-1290	Sand ridge, clinoforms
TP22-VC06	172	CERSA 1577	91.0 ± 31.5	0.92 ± 0.06	98.6 ± 34.7*	63900-133300	Deposits beneath the disconformity
TP22-VC07	184	CERSA 1200-20	0.78 ± 0.05	0.63 ± 0.05	1.24 ± 0.12	1120-1360	Sand ridge, buried clinoforms
TP22-VC07	204	CERSA 1200-22	0.72 ± 0.08	0.56 ± 0.04	1.30 ± 0.17	1130-1470	Sand ridge, buried clinoforms
TP22-VC24	100	CERSA 1578	0.43 ± 0.13	1.00 ± 0.04	0.43 ± 0.13	300-560	Deposits beneath the disconformity, offshore of the ridge
TP22-VC24	158	CERSA 1579	1.33 ± 0.06	1.01 ± 0.04	1.32 ± 0.08	1240-1400	Deposits beneath the disconformity,

https://doi.org/10.5194/egusphere-2026-2791
Preprint. Discussion started: 9 July 2026
© Author(s) 2026. CC BY 4.0 License.

							offshore of the ridge
TP22-VC25	185	CERSA 1580	0.43 ± 0.03	0.98 ± 0.04	0.44 ± 0.03	410-470	Sand ridge, clinoforms
TP22-VC26	108	CERSA 1199A	0.97 ± 0.19	1.16 ± 0.06	0.83 ± 0.17	660-1000	Sand ridge, clinoforms
TP22-VC26	113	CERSA 1199B	0.90 ± 0.11	0.91 ± 0.05	0.98 ± 0.13	850-1100	Sand ridge, clinoforms
TP22-VC26	126.5	CERSA 1199C	0.74 ± 0.07	0.85 ± 0.05	0.87 ± 0.10	770-970	Sand ridge, clinoforms
TP22-VC26	131.5	CERSA 1199D	0.78 ± 0.04	0.88 ± 0.05	0.89 ± 0.06	830-950	Sand ridge, clinoforms
TP22-VC26	142.5	CERSA 1199E	0.62 ± 0.11	0.62 ± 0.04	1.00 ± 0.19	810-1190	Sand ridge, gravel lag
TP22-VC26	153	CERSA 1199F	0.60 ± 0.05	0.56 ± 0.04	1.07 ± 0.12	950-1190	Sand ridge, gravel lag
TP22-VC26	165	CERSA 1199G	1.90 ± 0.56	0.51 ± 0.04	3.75 ± 1.16*	2590-4910	Sand ridge, gravel lag
TP22-VC26	180	CERSA 1199H	4.92 ± 0.21	0.95 ± 0.06	5.21 ± 0.38*	4830-5590	Deposits beneath the disconformity
TP22-VC26	187.5	CERSA 1199I	4.54 ± 0.59	0.97 ± 0.06	4.70 ± 0.67*	4030-5370	Deposits beneath the disconformity
TP22-VC26	203.5	CERSA 1199J	5.03 ± 0.14	0.97 ± 0.06	5.19 ± 0.37*	4820-5560	Deposits beneath the disconformity

Samples marked with * might contain reworked unbleached sand grains, and the age might be overestimated or with greater error. Additional information is included in Supplementary Material.

The deposits of the Stroombank sand ridge show broadly comparable ages in both the buried southwestern sector (e.g., TP22-VC07) and offshore of the ridge (e.g., TP22-VC06, TP22-VC26), with (OSL) ages ranging from 1130-1470 to 660-1000 a (Table 1, Fig. 6). Along a cross-shore transect (TP22-VC25 to TP22-VC04; transect B), ages decrease systematically towards the coast: TP22-VC25 yields an age of 410-470 a, while TP22-VC04 provides the youngest ridge age (170-230 a). The deeper basal sediments yield an older radiocarbon age of 490–705 cal a BP, consistent with the stratigraphic order (Table 1, Fig. 6). In this sector, core TP22-VC24, located offshore of the Stroombank, provided older ages for some of the deposits underlying the basal disconformity (Fig. 2B), 1260-1515 cal a BP and 1240-1400 a at the base (Table 1, Fig. 6). Towards the top of the core, the OSL age is similar to that of the ridge, 300-560 a (Table 1, Fig. 6).

A similar pattern is found in the Kleine Rede trough. Sandy deposits beneath the mud layer yield ages comparable to sand of the main ridge (440-2640 to 800-1380 a in TP22-VC03, Fig. 6), overlapping with ages for the gravelly basal unit in TP22-VC26 (950-1190 a, Fig. 6). In contrast, the overlying muds are significantly younger, with a radiocarbon age of 0–285 cal a BP (core TP22-VC03, Table 1, Fig. 6). Sediments overlying the buried southwestern portion of the Stroombank sand ridge,

https://doi.org/10.5194/egusphere-2026-2791
Preprint. Discussion started: 9 July 2026
© Author(s) 2026. CC BY 4.0 License.

representing the trough infilling that draped the ridge, are consistently young. Radiocarbon dates from marine shells indicate ages up to 660–915 cal a BP in TP23-VC45 (Figs. 3A and 6). Sediments directly overlying the buried ridge crest, such as found in TP23-VC47, yielded an age of 5–300 cal a BP (Figs. 2C and 6).

Collectively, these results indicate that the southwestern sector of the Stroombank contains the oldest ridge deposits. Ages progressively decrease landward and north-westward, a pattern that matches the luminescence-profiling trends.

5 Discussion

The integrated geophysical, sedimentological and chronological dataset presented in this study provides a robust basis for reconstructing the origin and long-term evolution of the Stroombank sand ridge and for evaluating its broader geomorphic significance. The discussion is structured in three parts. First, we reconstruct the evolutionary history of the ridge based on its internal architecture and chronological framework (Sect. 5.1). Second, we assess how these observations compare with existing models of SFCR formation and evolution (Sect. 5.2). Finally, we synthesise these findings into a process-based conceptual model that explains ridge initiation and elongation in the context of sediment supply, hydrodynamic forcing and coastal retreat (Sect. 5.3).

5.1 Origin and evolution of the Stroombank sand ridge

The stratigraphic architecture and chronological framework indicate that ridge evolution can be subdivided into two main development phases (Fig. 5B). Phase I corresponds to the initial construction and elongation of the ridge following its inception and is characterised by clinoformal units largely buried underneath younger aggrading and prograding deposits (Fig. 3). Phase II represents a subsequent stage of sustained accretion and internal reorganisation, marked by persistent landward-dipping clinoforms that form the present-day ridge morphology (Fig. 2). This two-phase framework provides a basis for reconstructing the timing and spatial evolution of the Stroombank.

The oldest (OSL) age obtained from ridge deposits of Phase I (1130-1470 a; TP22-VC07, Table 1, Fig. 6) indicates that ridge inception likely took place during the late Holocene, under relatively stable sea-level conditions (Denys and Baeteman, 1995). Phase I deposits directly overlie mid-Holocene sediments, as indicated by ages of 4820-5560 and 4030-5370 a obtained from sediments beneath the basal disconformity in core TP22-VC26 (Figs. 3C and 6). These data constrain the onset of the Stroombank development to ca. 1300 a (8th century CE) or slightly earlier. This timing excludes both a mid-Holocene origin inferred from analogies with the Dutch coast (Van Lancker, 1999) and a post-medieval formation proposed by Mathys (2009), therefore indicating that the Stroombank formed under near-modern boundary conditions.

The spatial distribution of the ridge is closely associated with Holocene tidal-inlet systems, with the Stroombank located between two relict inlets preserved at its southwestern and northeastern ends (Fig. 1) (Cartelle et al., 2025, 2026). The oldest ridge deposits occur in proximity to extensive tidal-delta sediments offshore of Nieuwpoort, suggesting a spatial and temporal link between inlet activity and ridge initiation. Chronological constraints indicate that inlet activity waned after ca.

https://doi.org/10.5194/egusphere-2026-2791
Preprint. Discussion started: 9 July 2026
© Author(s) 2026. CC BY 4.0 License.

1700 cal a BP (Cartelle et al., 2026), shortly preceding the timing of ridge inception. Sediments associated with this inlet system are preserved beneath and adjacent to the southwestern sector of the ridge and were affected by large-scale erosion (Figs. 1 and 3) prior to their burial under younger shoreface deposits. The overlap between the youngest ages of Phase I ridge deposits (660–780 a; TP22-VC05, Figs. 2A and 6) and the oldest ages of trough infill sediments (660–915 cal a BP; TP23-VC45, Figs. 3A and 6) indicates that both inlet-related deposits and the oldest sector of the ridge became buried at a similar time. Overall, this evidence suggests that ebb-tidal delta deposits may have acted as a short-lived but critical sediment reservoir that helped the onset of ridge formation and its elongation during Phase I.

Following the burial of the deltaic deposits and progressive infilling of the trough to the southwest, ridge development entered Phase II (Fig. 5B). This phase is characterised by a change in the availability of sediment sources, with ridge deposits overlying a substrate composed of discontinuous Holocene and Pleistocene units (Fig. 2). In the northeastern sector, high luminescence intensities and mud-rich intervals in the cores indicate the presence of these older deposits beneath a thin sediment veneer offshore of the ridge (e.g., TP22-VC24 and TP22-VC36-2, Figs. 2 and 6). The upper part of these deposits yielded younger ages comparable to those of the ridge (300-560 a, TP22-VC24, Figs. 2B and 6), indicating that they were reworked during later stages of ridge development. In addition, reconstructions of the late-Holocene coastline position indicate that the shoreface migrated landward across these existing deposits from a position at least ~2 km seaward of the present-day shoreline (Cartelle et al., 2026). The reconstructed palaeocoastline differs in orientation by approximately 5° from the modern coastline, closely matching the angular offset between Phase I and Phase II ridge deposits (Fig. 5), suggesting a link between coastline reorganisation and ridge geometry. Therefore, during Phase II, we interpret that ridge growth was sustained primarily through the reworking and recycling of these pre-existing shoreface deposits associated with continued coastal retreat and shoreface migration.

The chronological dataset reveals consistent spatial age patterns across the ridge that provide direct insight into its dynamics. Independently of the two-phase subdivision, ages systematically become younger from west to east along the ridge axis and from offshore to onshore across the ridge profile (Fig. 6). This spatial distribution of ages indicates progressive alongshore elongation combined with sustained landward migration of the sedimentary ridge through time. If the ridge originated ca. 1130-1470 a (720±170 CE) at the location of TP22-VC07 and connected to the coastline 8 km to the east of Oostende by the year 1866 CE (Dujardin et al., 2023), a distance of 25 km, this would represent an average alongshore elongation rate of ca. 1.9-2.5 km per century. This value integrates both Phase I and Phase II development and therefore represents a first-order estimate of long-term ridge growth rather than a phase-specific rate. Given the limited number of dated cores along the ridge axis, further subdivision of elongation rates between phases is not currently possible. The order of magnitude agrees well with estimations based on 200 years of bathymetric evolution reconstructed from historical charts (Dujardin et al., 2023, 2024; Houthuys et al., 2021), from which Houthuys et al. (2021) estimated an eastward migration rate of 1–2 km per century.

https://doi.org/10.5194/egusphere-2026-2791
Preprint. Discussion started: 9 July 2026
© Author(s) 2026. CC BY 4.0 License.

Cross-shore age differences provide additional constraints on landward-directed migration. For Phase I, comparison between TP22-VC26 and TP22-VC05, which are ca. 0.7 km apart (Fig. 3A) suggests landward migration rates in the order of ca. 400 m per century. During Phase II, age differences between TP22-VC25 and TP22-VC04 (Fig. 2B), across approximately 0.5 km of ridge width, indicate landward migration rates of ca. 200 m per century. These cross-shore distances were calculated by projecting dated clinoformal reflections along their apparent dip to the present seabed surface, thereby accounting for the internal geometry of the ridge rather than relying solely on horizontal core separation. Although simplified, these estimates are internally consistent and corroborate the persistent landward progradation recorded in the seismic architecture (Figs. 2, 3 and 5B).

In conclusion, the Stroombank records progressive late-Holocene ridge development characterised by northeastward elongation and sustained landward progradation since ca. 1300 a. Its internal architecture and chronological framework indicate that the present-day morphology resulted from two successive developmental phases: an initial stage linked to sediment supply from a waning tidal-inlet system, followed by prolonged ridge growth sustained through reworking and recycling of pre-existing shoreface deposits during continued coastal retreat and shoreface migration.

5.2 Implications for models of shoreface-connected ridge formation

The stratigraphic and chronological reconstruction of the Stroombank provides a rare opportunity to evaluate existing models of SFCR formation against a well-constrained, millennial-scale geological record. Most previous interpretations have relied primarily on morphology, surface sediments, or numerical modelling, whereas direct constraints on internal architecture and timing have remained limited. The Stroombank therefore offers a robust benchmark for assessing the applicability of these models.

Classical models for SFCR formation link ridge geometry and orientation to shoreline transgression and tidal-inlet retreat. In this framework, sand derived from ebb-tidal deltas is reworked during barrier retreat, and ridge orientation reflects the trajectory of migrating inlets and associated delta deposits (McBride and Moslow, 1991; Snedden et al., 1994). The Stroombank is partially consistent with this framework. The earliest phase of ridge development (Phase I) is spatially and temporally associated with a waning late-Holocene tidal inlet, indicating that inlet-derived sediment contributed to ridge initiation (Fig. 3). However, several key observations indicate that inlet retreat alone cannot explain the present configuration of the ridge. The Stroombank is oriented sub-parallel (ca. 8 degrees) to both the modern (Fig. 1) and late-Holocene (Cartelle et al., 2025, 2026) coastlines, rather than displaying the pronounced obliquity expected for features tracking inlet migration (ca. 25-35 degrees, Dyer and Huntley, 1999; McBride and Moslow, 1991; Snedden et al., 1994). In addition, the underlying stratigraphy shows no preserved evidence of a retreating tidal inlet or abandoned inlet channels but instead consists of a relatively uniform substrate of Palaeogene clays overlain by discontinuous Quaternary deposits (Figs. 2 and 3). Furthermore, the timing of ridge initiation during the late-Holocene highstand (Denys and Baeteman, 1995) excludes a

https://doi.org/10.5194/egusphere-2026-2791
Preprint. Discussion started: 9 July 2026
© Author(s) 2026. CC BY 4.0 License.

direct link with rapid transgressive phases. These observations suggest that inlet-derived sediment acted as an initial trigger rather than a sustained control on ridge development.

Comparison with process-based modelling studies also yields mixed agreement. Our reconstructions align with models of present-day hydrodynamics that emphasise NE-directed littoral transport driven by tidal asymmetry and flood-dominated currents (Dujardin et al., 2023), consistent with the observed alongshore elongation of the ridge. However, cross-shore transport remains under-resolved in some of these models, as the wave-driven component is only partially parameterised (Dujardin et al., 2023, 2024). Yet wave-mediated processes appear essential to explain the persistent landward migration imprinted in the internal structure of the Stroombank (Çiçek et al., 2026). Furthermore, our reconstructions diverge from the idealised morphodynamic models developed for shoreface-connected ridges (Calvete et al., 2001; Dujardin et al., 2024; van de Meene and van Rijn, 2000b; Nnafie et al., 2014, 2015, 2021, 2024; Trowbridge, 1995). These models predict seaward migration driven by offshore deflection of alongshore currents over the ridge crest and the loss of sediment-carrying capacity of the flow (Calvete et al., 2001; Trowbridge, 1995). Such behaviour fundamentally conflicts with the geological evidence from the Stroombank, which shows persistent and unequivocal landward migration since its inception.

The Stroombank also provides context for interpreting previous observations of ridge dynamics based on historical bathymetric datasets (Dujardin et al., 2023, 2024; Houthuys et al., 2021). While recent studies have suggested that landward migration may be driven by sea-level rise over decadal timescales (Nnafie et al., 2024), the geological record demonstrates that this behaviour has persisted for more than a millennium under relatively stable sea-level conditions. This indicates that landward migration is an intrinsic characteristic of the system rather than a short-term response to recent forcing.

Comparison with other documented SFCRs worldwide further contextualises these findings. In many regions, seismic data show limited internal stratification, providing little evidence for long-term migration (e.g., Parker et al., 1982; Schwab et al., 2000, 2013, 2014; Snedden et al., 1994; Swift and Field, 1981). An exception is the Sable Island system, where Dalrymple and Hoogendoorn (1997) observed large-scale seaward-dipping structures resembling migrating dunes. In contrast, the Stroombank displays a laterally continuous succession of landward-dipping clinoforms that clearly document persistent shoreward migration over centennial timescales. It is important to recognise that many earlier investigations predate the widespread use of very high-resolution sub-bottom profilers, and their datasets may not have been optimised to image fine-scale internal architecture. Consequently, the limited stratigraphic expression reported for other SFCRs may partly reflect differences in acquisition technology. Nonetheless, the Stroombank remains distinctive in the clarity and continuity of its internal architecture.

A common characteristic of many documented SFCRs worldwide is the presence of a distinct, relatively flat erosional surface forming their basal boundary (e.g., Dalrymple and Hoogendoorn, 1997; Goff, 2014; Schwab et al., 2000; Snedden et al., 1994). These disconformities are generally interpreted as ravinement surfaces generated by wave reworking or by erosion associated with ridge migration. The Stroombank displays a clear architectural similarity: a well-defined basal

https://doi.org/10.5194/egusphere-2026-2791
Preprint. Discussion started: 9 July 2026
© Author(s) 2026. CC BY 4.0 License.

disconformity separates the ridge deposits from underlying strata (Figs. 2 and 3). However, the morphology and sedimentological expression of this surface vary along the Stroombank and between developmental phases. In the southwestern sector, the basal surface associated with Phase I reaches depths of up to –20.2 m MSL and locally forms a relatively flat surface sloping to the southwest (Figs. 3, 4 and 5A). It is overlain by coarse lag deposits composed of gravel, shell fragments, sand and clay clasts (e.g., TP22-VC06, TP22-VC26; Figs. 6 and 7), indicative of high-energy reworking. These characteristics are consistent with ravinement-like erosion or a succession of energetic events during ridge initiation. By contrast, the basal contact associated with Phase II is more irregular (Fig. 5A) and lacks a distinctive coarse sedimentary signature in the available cores (Fig. 6), although sedimentological control in this sector remains limited. The Stroombank therefore shares the presence of a prominent basal erosional boundary with other SFCRs, but its geometry and sedimentary expression suggest a more complex, phase-dependent development rather than a single, regionally extensive ravinement surface.

Taken together, these observations indicate that existing conceptual and process-based models do not fully capture the mechanisms governing the formation and evolution of the Stroombank. In particular, they underestimate the role of evolving sediment supply and fail to reproduce the persistent landward migration recorded in the geological archive. Future modelling efforts should therefore focus on integrating geological boundary conditions, antecedent morphology, and dynamic sediment recycling into process-based simulations, while improving the representation of wave-driven cross-shore transport. The Stroombank provides a rare geological benchmark against which such models can now be evaluated.

5.3 Conceptual model for the formation and evolution of the Stroombank sand ridge

The observations presented in Sect. 5.1 and 5.2 can be integrated into a conceptual model that explains the initiation, elongation, and long-term migration of the Stroombank (Fig. 8). Ridge development is interpreted as a result of the combined influence of sediment supply, alongshore sediment transport, wave-driven cross-shore processes, and coastal retreat.

Ridge initiation was enabled by the availability of sediment derived from waning tidal-inlet and ebb-tidal-delta deposits in the southwestern sector of the study area (Figs. 1 and 8) (Cartelle et al., 2025, 2026). The progressive infilling and abandonment of the Nieuwpoort tidal inlet after ca. 1.7 cal ka BP removed an important hydrodynamic barrier and enabled sediment to be redistributed both alongshore by northeastern-directed currents and landward across the shoreface by wave-driven cross-shore transport. During this time, the late-Holocene coastline was located further seaward and displayed a slightly different orientation, bringing the zone of active sediment transport closer to the incipient ridge. These conditions favoured the initial accumulation and organisation of sediment into a ridge-like morphology (Fig. 8A). In this sense, ridge initiation reflects a combination of antecedent sediment availability and changes in boundary conditions, rather than a direct response to sea-level transgression.

https://doi.org/10.5194/egusphere-2026-2791
Preprint. Discussion started: 9 July 2026
© Author(s) 2026. CC BY 4.0 License.

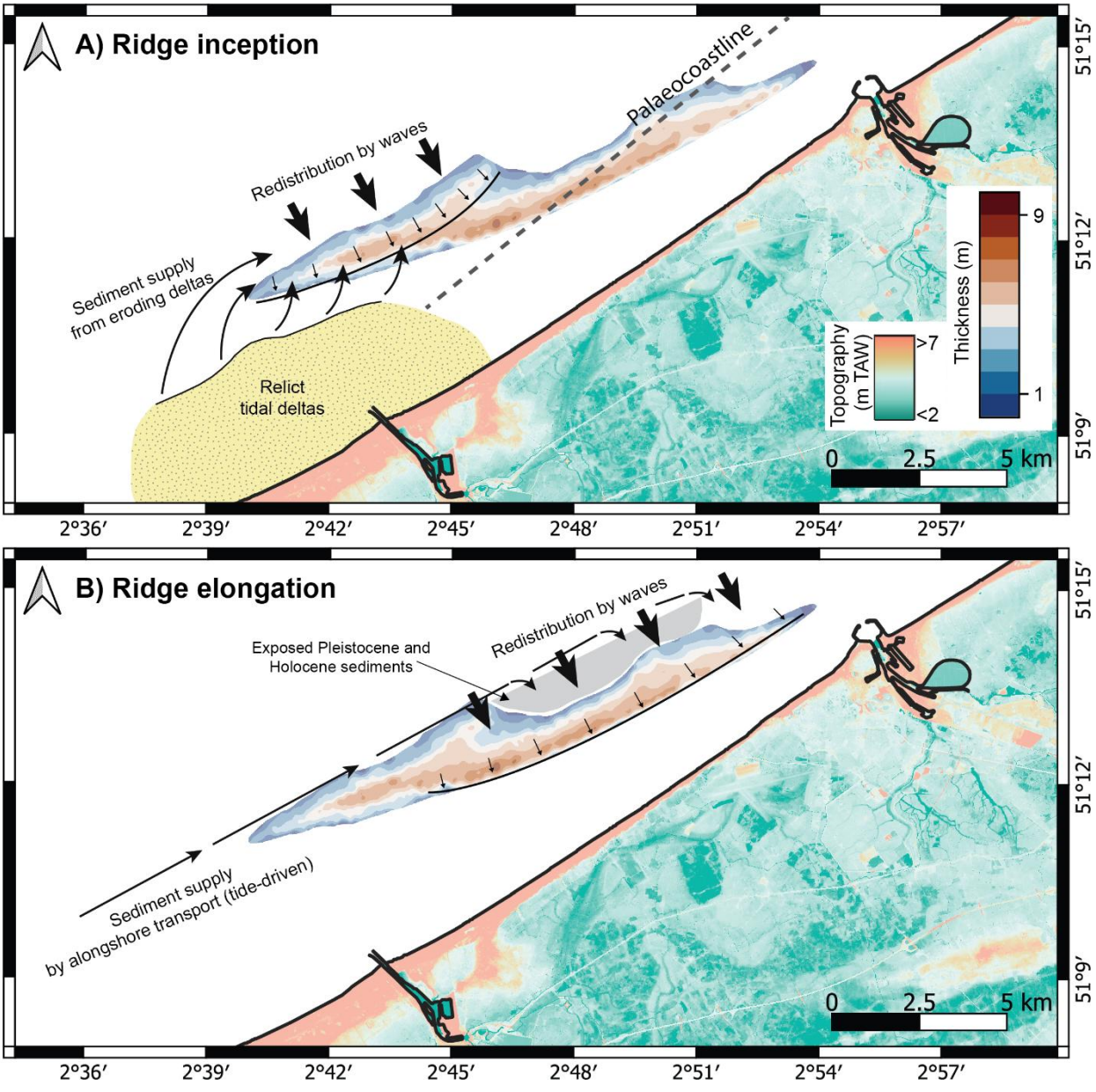

Figure 8. Conceptual model for the formation of the Stroombank sand ridge using the sediment thickness map of Fig. 5B. A) Ridge inception: the initial accumulation of sand was fuelled by sediment supplied from the erosion of relict tidal-delta deposits associated with a waning tidal-inlet system southwest of the Stroombank. This sediment was reworked and redistributed along the incipient ridge by wave-driven cross-shore transport. The palaeocoastline is based on the reconstructions of Cartelle et al. (2025, 2026) for the Late Holocene and represents a minimum seaward position. B) Ridge elongation: once the ebb-tidal-delta sediment source became buried, ridge development was maintained primarily by tide-driven alongshore sediment transport supplying sand from the southwest, and by wave-driven reworking that redistributed sediment across the ridge. Background topographic data were provided by Nationaal Geografisch Instituut and are available at www.geo.be.

https://doi.org/10.5194/egusphere-2026-2791
Preprint. Discussion started: 9 July 2026
© Author(s) 2026. CC BY 4.0 License.

Subsequent ridge evolution was governed by the interaction between alongshore and cross-shore sediment-transport processes (Fig. 8B). Alongshore transport, driven predominantly by flood-asymmetric tidal currents (Dujardin et al., 2023), supplied sediment from the southwest and controlled the progressive elongation of the ridge towards the northeast. At the same time, wave-driven processes redistributed sediment across the ridge, imposing a persistent landward transport component (Çiçek et al., 2026) that explains the observed progradation recorded in the clinoformal architecture (Fig. 2). The combined effect of these processes resulted in simultaneous alongshore extension and shoreward migration over centennial timescales. As the initial inlet-derived sediment source became progressively buried, ridge development was sustained through recycling of antecedent deposits within the shoreface. The landward migration of the coastline played a key role in this as the reworking of previously deposited Holocene and Pleistocene units allowed continued ridge accretion. The agreement between changes in coastline orientation and ridge geometry (both showing a ~5° change in orientation) further indicates that large-scale reorganisation of the coastal system influenced sediment-transport pathways and ridge development.

The relative contribution of storm-driven and fair-weather conditions in ridge evolution remains uncertain. Observations from comparable systems suggest that episodic, high-energy events may play a dominant role in sediment mobilisation and lower-shoreface morphodynamics (Calvete et al., 2001; Dalrymple and Hoogendoorn, 1997; Goff et al., 2015; Snedden et al., 2011), and a similar influence is likely for the Stroombank.

Although the role of coastal retreat is clearly reflected in the evolution of the Stroombank, the cause-and-effect relationship between ridge development and shoreline change remains uncertain. On the one hand, coastal retreat likely enhanced sediment availability through the erosion and reworking of tidal-inlet and shoreface deposits, thereby promoting ridge initiation and sustained accretion. On the other hand, the progressive elongation and landward migration of the ridge may have influenced sediment redistribution within the nearshore system, potentially affecting patterns of coastal erosion. The extent to which the Stroombank acted as a passive archive of changing sediment supply or as an active component in the morphodynamic evolution of the coastline cannot be resolved with the present dataset. This highlights the need for future studies integrating geological reconstructions with process-based modelling and shoreline-change analyses to better constrain the feedback between ridge dynamics and coastal evolution.

6 Conclusions

This study provides a detailed geological reconstruction of the Stroombank shoreface-connected ridge by integrating high-resolution geophysical data, sedimentological observations, and chronological constraints. The ridge is characterised by a well-defined internal architecture of landward-dipping clinoforms overlying an irregular basal disconformity that locally truncates Pleistocene and Holocene deposits. Chronological data indicate that ridge development began ca. 1.3 ka ago and has continued through sustained accretion and reorganisation.

https://doi.org/10.5194/egusphere-2026-2791
Preprint. Discussion started: 9 July 2026
© Author(s) 2026. CC BY 4.0 License.

The Stroombank records a two-phase evolutionary history. An initial phase of ridge formation was associated with sediment supplied from a waning late-Holocene tidal-inlet system, which acted as a transient but critical source during ridge inception. This was followed by a second phase in which ridge growth was maintained independently of the inlet through sediment redistribution within the active shoreface. The internal architecture and chronological framework further demonstrate consistent spatial trends, with progressive northeastward elongation and persistent landward migration over centennial timescales.

These results indicate that ridge evolution was governed by the combined influence of sediment supply, hydrodynamic forcing, and coastal retreat. The Stroombank therefore represents a composite geomorphic feature, in which antecedent conditions control initiation while ongoing processes sustain long-term development. The coexistence of preserved and active ridge domains highlights the spatial heterogeneity inherent to these systems and provides a unique geological record of their evolution. By providing robust chronostratigraphic constraints on ridge initiation and development, this study offers a geological benchmark against which existing conceptual and process-based models of shoreface-connected ridge formation and long-term evolution can be evaluated. More broadly, the results demonstrate the importance of integrating detailed geological reconstructions into the study of shoreface-connected ridges worldwide, particularly to assess the relative roles of antecedent morphology, sediment supply, and hydrodynamic forcing in controlling their long-term evolution.

Appendix A

Table A1. Metadata of the sediment cores selected for the present study, indicating survey, coordinates (WGS84), and length measured in the lab once split.

Core	Survey	Longitude (E)	Latitude (N)	Length (cm)
TP22-VC03	22-320	2.805553	51.20982498	236
TP22-VC04	22-320	2.8019393	51.21288891	232
TP22-VC05	22-320	2.75378931	51.20959627	5 (bagged)+186.5
TP22-VC06-1	22-320	2.69476833	51.19781995	185.5
TP22-VC07	22-320	2.68373041	51.18910589	21.5
TP22-VC24	22-380	2.79366417	51.22076969	213
TP22-VC25	22-380	2.79758606	51.21688434	218
TP22-VC26	22-380	2.74849191	51.21513078	221
TP22-VC27	22-380	2.69996705	51.20016017	219.5
TP22-VC28	22-380	2.69209055	51.19651461	216.5
TP22-VC29	22-380	2.68533868	51.18781551	208

https://doi.org/10.5194/egusphere-2026-2791
Preprint. Discussion started: 9 July 2026
© Author(s) 2026. CC BY 4.0 License.

TP22-36-2	22-380	2.84196629	51.23787001	189.5
TP22-VC37	23-220	2.84975938	51.23157607	216.5
TP22-VC38	23-220	2.85235537	51.22942327	186
TP23-VC45	23-220	2.682347189	51.17521359	225
TP23-VC46	23-220	2.683031398	51.18782934	190.5
TP23-VC47	23-220	2.702516998	51.19100556	185.5
TP23-VC48	23-220	2.887527724	51.2413837	170
TP23-VC49	23-220	2.891195658	51.23816848	242
TP24-VC50	24-320	2.829316595	51.21873916	95
TP24-VC51	24-320	2.830607745	51.21748087	237
TP23-VC55	23-220	2.724653366	51.19824143	161

Table A2. Sedimentary facies.

Facies	Description
Gravel facies	
mxd sG-m	Mixed (siliciclastic and bioclastic) matrix-supported gravel with a sand matrix. Matrix of medium sand, with a few cores with a coarse to very coarse sand matrix.
mxd msG-m	Mixed (siliciclastic and bioclastic) matrix-supported gravel with sand and mud matrix.
mxd sG-c	Mixed (siliciclastic and bioclastic) clast-supported gravel with a sand matrix.
Sand facies	
mS_{lam}	Laminated muddy sand. Siliciclastic. It may contain shells and shell fragments.
mS_{m}	Visually structureless muddy or slightly muddy siliciclastic sand which may contain some shells and shell fragments.
mS_{gr}	Finning upwards muddy or slightly muddy siliciclastic sand which may contain some shells and shell fragments.
S_{lam} $S_{lam\text{-}biot}$ $S_{lam\text{-}org}$	Laminated fine to medium sand with some shell fragments, it may include some thin mud laminae. Siliciclastic. Sometimes bioturbated (-biot), or organic rich (-org).

https://doi.org/10.5194/egusphere-2026-2791
Preprint. Discussion started: 9 July 2026
© Author(s) 2026. CC BY 4.0 License.

S_m $S_{m\text{-}gr}$	Visually structureless fine to medium sand with shell fragments. Siliciclastic. Sometimes finning upwards (-gr).
$S_{m\text{-}org}$	Visually structureless organic-rich fine to medium sand. Siliciclastic.
$mS_{m\text{-}rt\text{-}org}$ $mS_{m\text{-}rt\text{-}gr}$	Visually structureless muddy sand with root marks and organic fragments or lenses. No carbonate. Sometimes finning upwards (-gr).
mxd gS_{lam}	Mixed (bioclastic and siliciclastic) gravely medium or coarse sand, laminated.
mxd gS_m	Mixed (bioclastic and siliciclastic) gravely coarse to very coarse sand, visually structureless.
Mud facies	
C_m	Visually massive clay. Very stiff.
$sM_{lam\text{-}org}$	Organic-rich laminated sandy mud with some sand lenses and shell fragments.
$sM_{lam\text{-}org\text{-}biot}$	Laminated organic-rich sandy mud with some sand lenses and shell fragments. Bioturbated.
Heterolithic facies	
mS_{lam}/sM_m	Interbeds of laminated muddy fine to medium sand and visually structureless sandy mud.
$S_{lam}/M_{m\text{-}org}$	Interbeds of laminated fine to medium sand with shell fragments and organic-rich mud.
$S/M_{\ lam\text{-}biot}$ $M/S_{\ lam\text{-}biot}$	Interbeds of sand and mud. Sometimes bioturbated.
Other	
P	Peat, either in situ or transported.

https://doi.org/10.5194/egusphere-2026-2791
Preprint. Discussion started: 9 July 2026
© Author(s) 2026. CC BY 4.0 License.

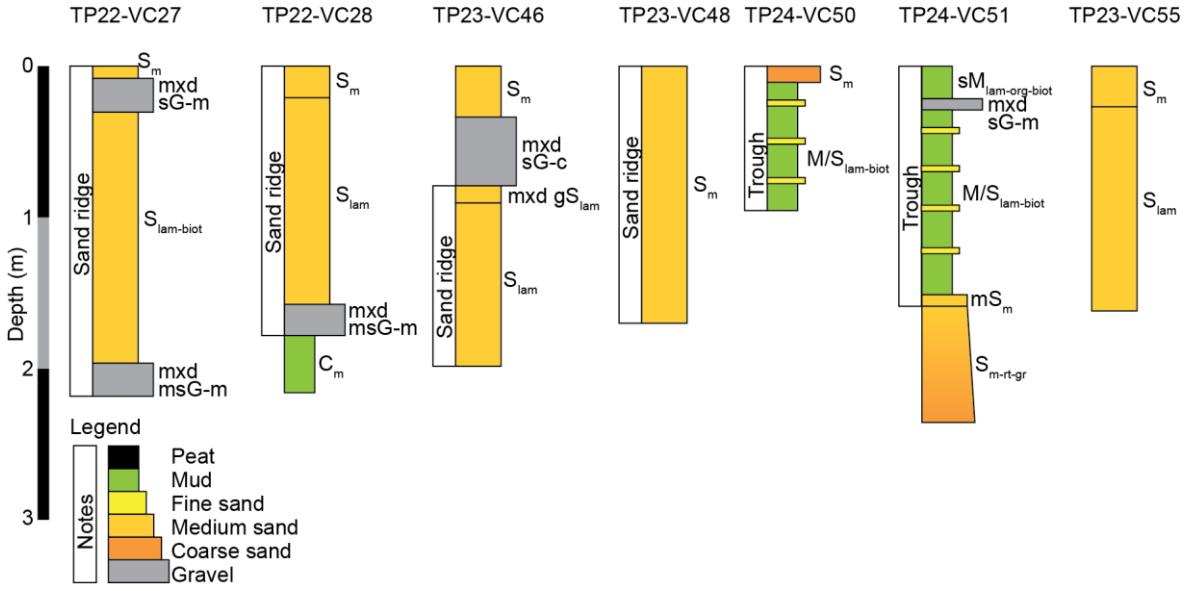

Figure A1. Core logs of sediment cores included in the study but not displayed in the main figures. Location is shown in Fig. 1C and sedimentary facies defined in Table A2.

Code and data availability

Upon publication, data will be made available in Marine Data Archive (https://marinedataarchive.org/) and the Integrated Marine Information System (https://vliz.be/en/imis) hosted by VLIZ.

Author contributions

Víctor Cartelle: Conceptualisation, Investigation, Formal analysis, Visualisation, Writing - Original Draft. **Soetkin Vervust**: Investigation, Writing - Review & Editing. **Thomas Mestdagh**: Investigation, Writing - Review & Editing. **Wout Van Wesemael**: Investigation, Writing - Review & Editing. **Yağız Arda Çiçek**: Writing - Review & Editing. **Christian Schwarz**: Writing - Review & Editing. **Tine Missiaen**: Writing - Review & Editing, Project administration, Funding acquisition. **Tim Kinnaird**: Investigation, Writing - Review & Editing. **Ruth Plets**: Conceptualisation, Writing - Review & Editing.

Competing interests

Some authors are members of the editorial board of journal *Earth Surface Dynamics*.

https://doi.org/10.5194/egusphere-2026-2791
Preprint. Discussion started: 9 July 2026
© Author(s) 2026. CC BY 4.0 License.

Acknowledgements

This study was carried out within the project: 'TESTEREP: The evolution of the Flemish coastal seascape (5000 BP-present) - Testerep reconstructed for policymaking and the public engagement', part of the Strategic Basic Research (SBO) program of the Fund for Scientific Research (FWO). It ran from 1 October 2021 to 30 September 2025 (Ref. S007522N). The crew of RV *Simon Stevin* and DAB Vloot and the crew of the *Last Freedom* are acknowledged for their support in performing the research at sea. Our special thanks go to Jan Vermaut and Wouter Blomme, whose skilled technical support during the offshore coring operations greatly contributed to the success of this study. The authors thank Jaak Monbaliu and Marc de Bie for their contributions to earlier stages of this work.

References

Anthony, E. J. and Aagaard, T.: The lower shoreface: Morphodynamics and sediment connectivity with the upper shoreface and beach, Earth-Science Reviews, 210, 103334, https://doi.org/10.1016/j.earscirev.2020.103334, 2020.

Antia, E. E.: Shoreface-Connected Ridges in German and U.S. Mid-Atlantic Bights: Similarities and Contrasts, Journal of Coastal Research, 12, 141–146, 1996.

Calvete, D., Falques, A., De Swart, H. E., and Walgreen, M.: Modelling the formation of shoreface-connected sand ridges on storm-dominated inner shelves, J. Fluid Mech., 441, 169–193, https://doi.org/10.1017/S0022112001004815, 2001.

Cartelle, V., Plets, R., Çiçek, Y. A., Schwarz, C., Monbaliu, J., Missiaen, T., Vanbiervliet, Z., and Vervust, S.: From field data to model: integration of onshore and offshore research to create a Digital Terrain Model of the Belgian coast around 6 ka BP for geoarchaeological research, ArcheoSciences, 49, 377–380, https://doi.org/10.4000/14nt2, 2025.

Cartelle, V., Vervust, S., Van Wesemael, W., Mestdagh, T., Çiçek, Y. A., Schwarz, C., Missiaen, T., De Bie, M., and Plets, R.: Corrigendum to “Advantages of integrated geophysical, sedimentary, and dating approaches for reconstructing Holocene tidal inlet evolution: A case study from offshore the Belgian coastal plain” [Geomorphology 505 (2026) 110311], Geomorphology, 506, 110332, https://doi.org/10.1016/j.geomorph.2026.110332, 2026.

Cawthra, H. C., Neumann, F. H., Uken, R., Smith, A. M., Guastella, L. A., and Yates, A.: Sedimentation on the narrow (8 km wide), oceanic current-influenced continental shelf off Durban, KwaZulu-Natal, South Africa, Marine Geology, 323–325, 107–122, https://doi.org/10.1016/j.margeo.2012.08.001, 2012.

Çiçek, Y. A., Monbaliu, J., Toorman, E., Cartelle, V., Plets, R., Pil, N., Vervust, S., and Schwarz, C.: Optimizing Long-Term Morphodynamic Predictions in Response to Dominant Forcing: A Case Study on the Belgian Continental Shelf., Coastal Engineering, 104989, https://doi.org/10.1016/j.coastaleng.2026.104989, 2026.

Dalrymple, R. W. and Hoogendoorn, E. L.: Erosion and Deposition on Migrating Shoreface-attached Ridges, Sable Island, Eastern Canada, Geoscience Canada, 1997.

De Batist, M.: Seismostratigrafie en structuur van het Paleogeen in de Zuidelijke Noordzee., University of Gent, 107 pp., 1989.

https://doi.org/10.5194/egusphere-2026-2791
Preprint. Discussion started: 9 July 2026
© Author(s) 2026. CC BY 4.0 License.

De Clercq, M.: Drowned landscapes of the Belgian Continental Shelf: implications for northwest European landscape evolution and preservation potential for submerged heritage, Ghent University, Belgium, 353 pp., 2018.

De Clercq, M., Chademenos, V., Van Lancker, V., and Missiaen, T.: A high-resolution DEM for the Top-Palaeogene surface of the Belgian Continental Shelf, Journal of Maps, 12, 1047–1054, https://doi.org/10.1080/17445647.2015.1117992, 2016.

Denys, L. and Baeteman, C.: Holocene evolution of relative sea level and local mean high water spring tides in Belgium—a first assessment, Marine Geology, 124, 1–19, https://doi.org/10.1016/0025-3227(95)00029-X, 1995.

Dujardin, A., Houthuys, R., Nnafie, A., Röbke, B., van der Werf, J., de Swart, H. E., Biernaux, H. E., De Maerschalck, B., Dan, S., and Verwaest, T.: MOZES – Research on the Morphological Interaction between the Sea bottom and the Belgian Coastline. Working year 1., Flanders Hydraulics, Antwerp, 2023.

Dujardin, A., Houthuys, R., Nnafie, A., van der Werf, J., de Swart, H. E., Biernaux, V., De Maerschalck, D., Dan, S., and Verwaest, T.: MOZES – Research on the Morphological Interaction between the Sea bottom and the Belgian Coastline. Working year 2., Flanders Hydraulics, Antwerp, 2024.

Dyer, K. R. and Huntley, D. A.: The origin, classification and modelling of sand banks and ridges, Cont. Shelf Res., 19, 1285–1330, https://doi.org/10.1016/S0278-4343(99)00028-X, 1999.

Farrell, K. M., Harris, W. B., Mallinson, D. J., Culver, S. J., Riggs, S. R., Pierson, J., Self-Trail, J. M., and Lautier, J. C.: Standardizing Texture and Facies Codes for A Process-Based Classification of Clastic Sediment and Rock, Journal of Sedimentary Research, 82, 364–378, https://doi.org/20120626195552, 2012.

Goff, J. A.: Seismic and core investigation off Panama City, Florida, reveals sand ridge influence on formation of the shoreface ravinement, Continental Shelf Research, 88, 34–46, https://doi.org/10.1016/j.csr.2014.07.006, 2014.

Goff, J. A., Flood, R. D., Austin, Jr., James A., Schwab, W. C., Christensen, B., Browne, C. M., Denny, J. F., and Baldwin, W. E.: The impact of Hurricane Sandy on the shoreface and inner shelf of Fire Island, New York: Large bedform migration but limited erosion, Continental Shelf Research, 98, 13–25, https://doi.org/10.1016/j.csr.2015.03.001, 2015.

Heaton, T. J., Köhler, P., Butzin, M., Bard, E., Reimer, R. W., Austin, W. E. N., Bronk Ramsey, C., Grootes, P. M., Hughen, K. A., Kromer, B., Reimer, P. J., Adkins, J., Burke, A., Cook, M. S., Olsen, J., and Skinner, L. C.: Marine20 - The Marine Radiocarbon Age Calibration Curve (0-55,000 cal BP), Radiocarbon, 62, 779–820, https://doi.org/10.1017/RDC.2020.68, 2020.

Henriet, J. P. and De Moor, G.: The Quaternary and Tertiary geology of the Southern Bight, North Sea, 241 pp., 1989.

Hequette, A. and Aernouts, D.: The influence of nearshore sand bank dynamics on shoreline evolution in a macrotidal coastal environment, Calais, northern France, Continental Shelf Research, 30, 1349–1361, https://doi.org/10.1016/j.csr.2010.04.017, 2010.

Houthuys, R., Vos, G., Dan, S., and Verwaest, T.: Long-term morphological evolution of the Flemish coast, Flanders Hydraulics, Antwerp, 2021.

Jacobs, P. and De Batist, M.: Sequence stratigraphy and architecture on a ramp-type continental shelf: the Belgian Palaeogene, SP, 117, 23–48, https://doi.org/10.1144/GSL.SP.1996.117.01.03, 1996.

https://doi.org/10.5194/egusphere-2026-2791
Preprint. Discussion started: 9 July 2026
© Author(s) 2026. CC BY 4.0 License.

Kana, T. W., Rosati, J. D., and Traynum, S. B.: Lack of evidence for onshore sediment transport from deep water at decadal time scales: Fire Island, New York, in: J. Coast. Res., Journal of Coastal Research, journalAbbreviation: J. Coast. Res., 61–75, https://doi.org/10.2112/SI59-007.1, 2011.

Mathys, M.: The Quaternary geological evolution of the Belgian Continental Shelf, southern North Sea, Ghent University, Belgium, 382 pp., 2009.

McBride, R. A. and Moslow, T. F.: Origin, evolution, and distribution of shoreface sand ridges, Atlantic inner shelf, U.S.A., Marine Geology, 97, 57–85, https://doi.org/10.1016/0025-3227(91)90019-Z, 1991.

van de Meene, J. W. H. and van Rijn, L. C.: The shoreface-connected ridges along the central Dutch coast — part 1: field observations, Continental Shelf Research, 20, 2295–2323, https://doi.org/10.1016/S0278-4343(00)00048-0, 2000a.

van de Meene, J. W. H. and van Rijn, L. C.: The shoreface-connected ridges along the central Dutch coast — part 2: morphological modelling, Continental Shelf Research, 20, 2325–2345, https://doi.org/10.1016/S0278-4343(00)00049-2, 2000b.

Missiaen, T., Evangelinos, D., Claerhout, C., De Clercq, M., Pieters, M., and Demerre, I.: Archaeological prospection of the nearshore and intertidal area using ultra-high resolution marine acoustic techniques: Results from a test study on the Belgian coast at Ostend-Raversijde, Geoarchaeology, 33, 386–400, https://doi.org/10.1002/gea.21656, 2018.

Mitchum, R. M. Jr.: Seismic Stratigraphy and Global Changes of Sea Level, Part 11: Glossary of Terms used in Seismic Stratigraphy, in: Seismic Stratigraphy – Applications to Hydrocarbon Exploration, American Association of Petroleum Geologists Memoir 26, edited by: Payton, C. E., 135–144, https://doi.org/10.1306/M26490C13, 1977.

Mitchum, R. M. Jr. and Vail, P. R.: Seismic Stratigraphy and Global Changes of Sea Level, Part 7: Seismic Stratigraphic Interpretation Procedure, in: Seismic Stratigraphy – Applications to Hydrocarbon Exploration, American Association of Petroleum Geologists Memoir 26, edited by: Payton, C. E., 135–144, 1977.

Mitchum, R. M. Jr., Vail, P. R., and Samgree, J. B.: Seismic Stratigraphy and Global Changes of Sea Level, Part 6: Stratigraphic interpretation of seismic reflections patterns in depositional sequences, in: Seismic Stratigraphy – Applications to Hydrocarbon Exploration, American Association of Petroleum Geologists Memoir 26, edited by: Payton, C. E., 117–133, 1977.

Muñoz, A., Acosta, J., Cristobo, J., Druet, M., and Uchupi, E.: Geomorphology and shallow structure of a segment of the Atlantic Patagonian margin, Earth-Science Reviews, 121, 73–95, https://doi.org/10.1016/j.earscirev.2013.03.002, 2013.

Munyikwa, K., Kinnaird, T. C., and Sanderson, D. C. W.: The potential of portable luminescence readers in geomorphological investigations: a review, Earth Surf Processes Landf, 46, 131–150, https://doi.org/10.1002/esp.4975, 2021.

Nnafie, A., de Swart, H. E., Calvete, D., and Garnier, R.: Effects of sea level rise on the formation and drowning of shoreface-connected sand ridges, a model study, Continental Shelf Research, 80, 32–48, https://doi.org/10.1016/j.csr.2014.02.017, 2014.

https://doi.org/10.5194/egusphere-2026-2791
Preprint. Discussion started: 9 July 2026
© Author(s) 2026. CC BY 4.0 License.

Nnafie, A., Swart, H. E. de, Calvete, D., and Garnier R.: Dynamics of shoreface-connected and inactive sand ridges on a shelf, Part 2: The role of sea level rise and associated changes in shelf geometry, Continental Shelf Research, 104, 63–75, https://doi.org/10.1016/j.csr.2015.05.009, 2015.

Nnafie, A., de Swart, H. E., Falqués, A., and Calvete, D.: Long-Term Morphodynamics of a Coupled Shelf-Shoreline System Forced by Waves and Tides, a Model Approach, Journal of Geophysical Research: Earth Surface, 126, e2021JF006315, https://doi.org/10.1029/2021JF006315, 2021.

Nnafie, A., de Swart, H. E., Boersma, J. M., Verwaest, T., Falqués, A., and Calvete, D.: Presence and Position of Sand Ridges on the Shelf Strongly Impact Decadal Evolution of Adjacent Shorelines: A Model Study, Journal of Geophysical Research: Earth Surface, 129, e2024JF007814, https://doi.org/10.1029/2024JF007814, 2024.

Parker, G., Lanfredi, N. W., and Swift, D. J. P.: Seafloor response to flow in a southern hemisphere sand-ridge field: Argentine inner shelf, Sedimentary Geology, 33, 195–216, https://doi.org/10.1016/0037-0738(82)90055-0, 1982.

Pendleton, E. A., Brothers, L. L., Thieler, E. R., and Sweeney, E. M.: Sand ridge morphology and bedform migration patterns derived from bathymetry and backscatter on the inner-continental shelf offshore of Assateague Island, USA, Continental Shelf Research, 144, 80–97, https://doi.org/10.1016/j.csr.2017.06.021, 2017.

Reimer, P. J., Austin, W. E. N., Bard, E., Bayliss, A., Blackwell, P. G., Ramsey, C. B., Butzin, M., Cheng, H., Edwards, R. L., Friedrich, M., Grootes, P. M., Guilderson, T. P., Hajdas, I., Heaton, T. J., Hogg, A. G., Hughen, K. A., Kromer, B., Manning, S. W., Muscheler, R., Palmer, J. G., Pearson, C., Plicht, J. van der, Reimer, R. W., Richards, D. A., Scott, E. M., Southon, J. R., Turney, C. S. M., Wacker, L., Adolphi, F., Büntgen, U., Capano, M., Fahrni, S. M., Fogtmann-Schulz, A., Friedrich, R., Köhler, P., Kudsk, S., Miyake, F., Olsen, J., Reinig, F., Sakamoto, M., Sookdeo, A., and Talamo, S.: The IntCal20 Northern Hemisphere Radiocarbon Age Calibration Curve (0–55 cal kBP), Radiocarbon, 62, 725–757, https://doi.org/10.1017/RDC.2020.41, 2020.

Safak, I., List, J. H., Warner, J. C., and Schwab, W. C.: Persistent Shoreline Shape Induced From Offshore Geologic Framework: Effects of Shoreface Connected Ridges, Journal of Geophysical Research: Oceans, 122, 8721–8738, https://doi.org/10.1002/2017JC012808, 2017.

Sanderson, D. C. W. and Murphy, S.: Using simple portable OSL measurements and laboratory characterisation to help understand complex and heterogeneous sediment sequences for luminescence dating, Quaternary Geochronology, 5, 299–305, https://doi.org/10.1016/j.quageo.2009.02.001, 2010.

Schwab, W. C., Thieler, E. R., Allen, J. R., Foster, D. S., Swift, B. A., and Denny, J. F.: Influence of Inner-Continental Shelf Geologic Framework on the Evolution and Behavior of the Barrier-Island System between Fire Island Inlet and Shinnecock Inlet, Long Island, New York, Journal of Coastal Research, 16, 408–422, 2000.

Schwab, W. C., Baldwin, W. E., Hapke, C. J., Lentz, E. E., Gayes, P. T., Denny, J. F., List, J. H., and Warner, J. C.: Geologic Evidence for Onshore Sediment Transport from the Inner Continental Shelf: Fire Island, New York, Journal of Coastal Research, 29, 526–544, https://doi.org/10.2112/JCOASTRES-D-12-00160.1, 2013.

https://doi.org/10.5194/egusphere-2026-2791
Preprint. Discussion started: 9 July 2026
© Author(s) 2026. CC BY 4.0 License.

Schwab, W. C., Baldwin, W. E., Denny, J. F., Hapke, C. J., Gayes, P. T., List, J. H., and Warner, J. C.: Modification of the Quaternary stratigraphic framework of the inner-continental shelf by Holocene marine transgression: An example offshore of Fire Island, New York, Marine Geology, 355, 346–360, https://doi.org/10.1016/j.margeo.2014.06.011, 2014.

Snedden, J. W., Tillman, R. W., Kreisa, R. D., Schweller, W. J., Culver, S. J., and Winn, R. D.: Stratigraphy and Genesis of a Modern Shoreface-Attached Sand Ridge, Peahala Ridge, New Jersey, SEPM JSR, 64, https://doi.org/10.1306/D4268004-2B26-11D7-8648000102C1865D, 1994.

Snedden, J. W., Tillman, R. W., and Culver, S. J.: Genesis and Evolution of a Mid-Shelf, Storm-Built Sand Ridge, New Jersey Continental Shelf, U.S.A., Journal of Sedimentary Research, 81, 534–552, https://doi.org/20110630160541, 2011.

Stuiver, M. and Reimer, P. J.: Extended 14C Data Base and Revised CALIB 3.0 14C Age Calibration Program, Radiocarbon, 35, 215–230, https://doi.org/10.1017/S0033822200013904, 1993.

Swift, D. J. P. and Field, M. E.: Evolution of a classic sand ridge field: Maryland sector, North American inner shelf, Sedimentology, 28, 461–482, https://doi.org/10.1111/j.1365-3091.1981.tb01695.x, 1981.

Swift, D. J. P., Parker, G., Lanfredi, N. W., Perillo, G., and Figge, K.: Shoreface-connected sand ridges on American and European shelves: A comparison, Estuarine and Coastal Marine Science, 7, 257–273, https://doi.org/10.1016/0302-3524(78)90109-3, 1978.

Trowbridge, J. H.: A mechanism for the formation and maintenance of shore-oblique sand ridges on storm-dominated shelves, Journal of Geophysical Research: Oceans, 100, 16071–16086, https://doi.org/10.1029/95JC01589, 1995.

Van Lancker, V. R. M.: Sediment and morphodynamics of a siliciclastic near coastal area, in relation to hydrodynamical and meteorological conditions: Belgian Continental Shelf, University of Gent, Gent, 201 pp., 1999.

Verwaest, T., Houthuys, R., Roest, B., Dan, S., and Montreuil, A.-L.: A Coastline Perturbation caused by Natural Feeding from a Shoreface-connected Ridge (Headland Sint-André, Belgium), Journal of Coastal Research, 95, 701, https://doi.org/10.2112/SI95-136.1, 2020.

Verwaest, T., Dujardin, A., Montreuil, A.-L., and Trouw, K.: Understanding Coastal Resilience of the Belgian West Coast, Water, 14, 2104, https://doi.org/10.3390/w14132104, 2022.

Wentworth, C. K.: A Scale of Grade and Class Terms for Clastic Sediments, J. Geol., 30, 377–392, https://doi.org/10.1086/622910, 1922.